Photoswitching of Bis-Spiropyran Using Upconversion Luminescent Tm^{3+}/Yb^{3+}-Co-Doped Lithium Yttrium Fluoride Nanoparticles

Biao Fei Zhang

A Thesis

in

The Department

Of

Chemistry and Biochemistry

Presented in Partial Fulfillment of the Requirements

for the Degree of Master of Science (Chemistry) at

Concordia University

Montreal, Quebec, Canada

February, 2013

CONCORDIA UNIVERSITY
School of Graduate Studies

This is to certify that the thesis prepared

By: **Biao Fei Zhang**

Entitled: **Photoswitching of Bis-Spiropyran Using Upconversion Luminescent Tm^{3+}/Yb^{3+}-Co-Doped Lithium Yttrium Fluoride Nanoparticles**

And submitted in partial fullfillment of the requirements for the degree of

Master of Science (Chemistry)

Complies with the regulations of the University and meets the accepted standards with respect to originality and quality.

Signed by the final examining committee:

_____ Chair
Dr. Dajana Vuckovic

_____ Examiner
Dr. P. H. Bird

_____ Examiner
Dr. L.A. Cuccia

_____ Supervisor
Dr. J. A. Capobianco

Approved by _____
Chair of Department or Graduate Program Director

_____
Dean, Faculty of Arts and Science

Date February 27, 2013

ABSTRACT

Photoswitching of Bis-Spiropyran Using Upconversion Luminescent Tm^{3+}/Yb^{3+}-Co-Doped Lithium Yttrium Fluoride Nanoparticles

Biao Fei Zhang

This thesis presents the synthesis and optical studies of a photoswitching model system, which consists of the lanthanide-doped upconversion luminescent nanoparticles (UCNPs) and photochromic bis-spiropyrans (BSPs).

The thermal decomposition synthetic strategy was employed to prepare monodisperse upconversion luminescent $LiYF_4$ (Y^{3+} 74.5 mol %, Tm^{3+} 0.5 mol %, and Yb^{3+} 25 mol %) nanoparticles (UCNPs), using the optimized conditions established; a reaction temperature of 315 ºC, reaction time of 90 minutes, and an injection rate of 1.5 mL/min for precursor addition. The as-prepared UCNPs were fully characterized using X-ray powder diffraction (XRPD), Fournier transform infrared spectroscopy (FTIR), transmission electron microscopy (TEM), and upconversion (UC) fluorescence emission spectroscopy.

Following a ligand exchange process, bis-spiropyran (BSP) was grafted on the surface of the UCNPs by replacing the oleate molecules. The BSP-UCNPs construct was investigated and we demonstrated the photoswitching of bis-spiropyran in this new system. Photoswitching occurs *via* fluorescence resonance energy transfer (FRET) from the UCNPs to bis-spiropyran.

We also explored the energy transfer efficiency between the UCNPs and ring-closed bis-spiropyran molecule and carried out a kinetic study of the photoswitching from

ring-closed colorless bis-spiropyran to ring-open colored bis-merocyanine, as well as the photodegradation of the bis-spiropyran functionalized UCNPs.

Taking advantage of the high penetration depth, reduced photodamage, and minimal autofluorescence of the NIR light excitation, this model system could be useful in biological applications related to photoswitching of photochromic compounds which requires UV irradiation to achieve the photochromic transformation.

ACKNOWNOLEDGEMENTS

I would like to express my extreme gratitude to my supervisor, Professor John A. Capobianco for giving me the opportunity to conduct my master's research project, and for his continuous support and guidance. Without your dedication and guidance, my thesis would never have been published.

I would like to sincerely and wholeheartedly thank Professor Fiorenzo Vetrone, Institut National de la Recherche Scientifique – Énergie, Matériaux et Télécommunications, Université du Québec for his guidance and helpful suggestions.

I would like to sincerely express my appreciation to my collaborator, Dr. Michel Frigoli, from Institut Lavoisier, Université de Versailles Saint-Quentin-en-Yvelines, for preparing the bis-spiropyan and helpful suggestions. I would also like to thank Fabio Angiuli from Università degli Studi di Parma, for his scientific insights, and I really cherish the summer we spent doing research.

To the members of my research committee, Prof. Peter Bird and Prof. Louis Cuccia, I wish to express my thanks and appreciation for your encouragement and support throughout the course of this degree and for serving on my thesis committee.

From the bottom of my heart, I thank the current members of the Lanthanide Research Group, Dr. Rafik Naccache, and Dr. Nicoleta Bogdan, who continued offering me their generous help, sage advice and good leads, and without which I could not have finished my project. The experience that they shared with me gives me an added confidence and makes me more a more complete researcher.

I would also like to thank other members and colleagues in the Capobianco lab who have taught me much, and for their precious time and generous help.

I wholeheartedly acknowledge Professor Laszlo Kalman for allowing to use his laboratory facilities and his helpful suggestions. I must also express my gratitude to Sasmit Deshmukh for his generous help in setting the apparatus in Professor Kalman's lab.

I would like to thank my wife for her everlasting love and support. You are always there to encourage me in my difficult time.

I would like to acknowledge the Natural Sciences and Engineering Research Council (NSERC) of Canada, and Concordia University for funding. I am grateful les Fonds Québécois de Recherche sur la Nature et les Technologies (FQRNT) for financial support through the FQRNT Scholarship Program.

Table of Contents

LIST OF FIGURES

CONTRIBUTIONS OF AUTHORS

The following summarizes the contributions of each of the authors cited in this thesis.

B. F. Zhang: experimental work and manuscript preparation

M. Frigoli: Bis-spiropyran preparation

F. Angiuli, aided in experimental work

F. Vetrone: aided in experimental work

J. A. Capobianco: project supervisor

Chapter One - Introduction

1.1. Photochromism

The first report of photochromism was given by Fritzsche in 1867, who observed the bleaching of an orange-colored solution of tetracene in daylight and the regeneration of the color in the dark. Later, more photochromic phenomena were observed and reported such as a color change of the potassium salt of dinitroethane in the solid state by ter Meer. Phipson observed that a gate post painted with a zinc pigment appeared black in daylight and white at night. Since that time interest in photochromism has continued. In 1950, Hirshberg investigated the mechanisms and the synthesis of compounds, which showed this phenomenon, and suggested the term "photochromism" [from the Greek words: phos (light) and chroma (color)] to describe his observations [1-3].

1.1.1. Definition of Photochromism

Photochromism is defined as a reversible transformation of a chemical species between two states, induced by irradiating with different wavelength of light [3, 4]. The two isomers exhibit distinct colours and thus have distinct absorption spectra respectively.

Figure 1. 1. Schematic of Photochromism

As shown in Figure 1.1, the thermodynamically stable colorless form A is transformed to the colored form B upon irradiation of a specific wavelength of light $h\nu_1$. The reverse process can occur thermally or under light illumination of $h\nu_2$ [4].

In general, photochromism requires that: (i) two the states of the molecule be thermally stable for a reasonable length of time at ambient temperature, (ii) the color change of the two states should be apparent by eye; and (iii) that the reaction be reversible. Irreversible photochemistry reactions are excluded [3].

Photochromism can occur in both inorganic and organic compounds, as well as in biological systems [5]. Among inorganic compounds, some metal oxides, alkaline earth sulfides, titanates, metal halides, and some transition metal compounds exhibit photochromism. One of the well-known photochromic inorganic compounds is silver halide which is used in the manufacture of photochromic lenses [3-5].

Many organic compounds, such as some anilines, disulfoxides, hydroazones, osazones, semicarbazones, stilbene derivatives, succinic anhydride, camphor derivatives, o-nitrobenzyl derivatives, and spiro compounds, show photochromism [2, 5]. The photochromic process in the previously mentioned compounds can be activated by ultraviolet and visible light. For example, under UV irradiation, colorless spiropyran can be transformed to merocyanine which is pink, in turn, merocyanine can be switched back to spiropyran upon illuminating with visible light (Figure 1.2) [6].

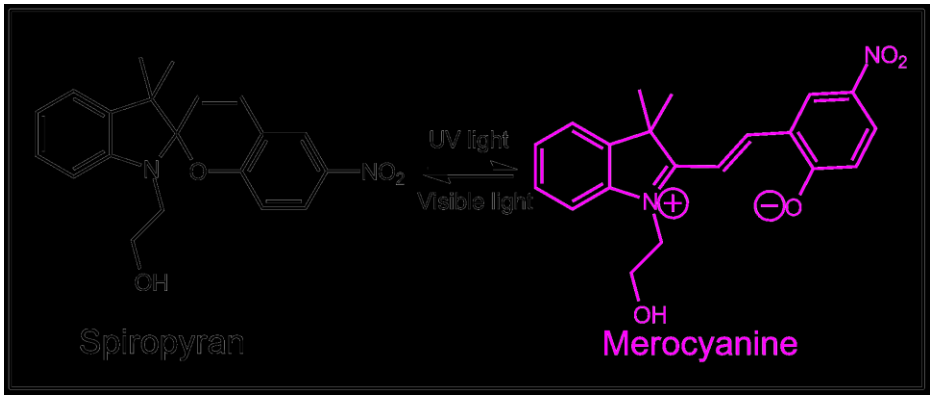

Figure 1. 2. Schematic photochromism of spiropyran

Owing to the convenience of obtaining a photochromic response in a wide range of wavelengths, organic photochromic compounds have been studied extensively. Organic photochromic compounds show great flexibility in structural modification, which renders them versatile for a myriad of different applications [5].

1.1.2. Classification of Organic Photochromic Compounds

To date, more than one hundred organic photochromic molecules have been developed. The most commonly known organic photochromic families include spiropyrans, spirooxanines, diarylethenes, and azobenzenes [2-5]. Their photochromic processes involve different chemical reactions, such as heterolytic cleavage, photocyclization, and trans-cis isomerization, etc. Table 1.1 illustrates the structural changes, which occur in these different families of compounds during the photochromic process.

In general, the appearance of a specific color is produced by irradiation with ultraviolet light. Both spiropyrans and spirooxanines experience a heterolytic cleavage reaction when irradiated with UV light; whereas, diarylethenes undergo photocyclization reaction, and azobezenes show trans-cis isomerization.

Table 1.1: Stuctures in the photochromism of spiropyrans, spirooxazines, diarylethenes and azobezenes.

Spiropyrans	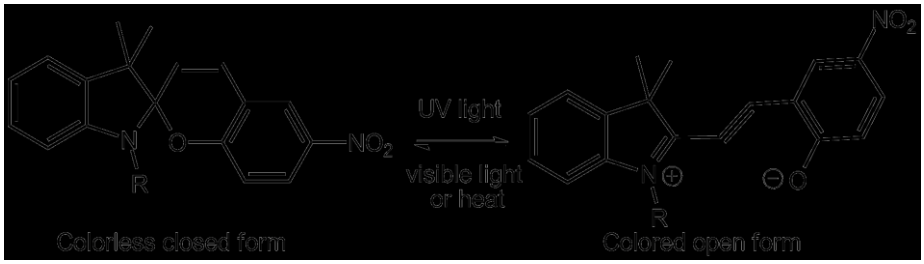
Spirooxanines	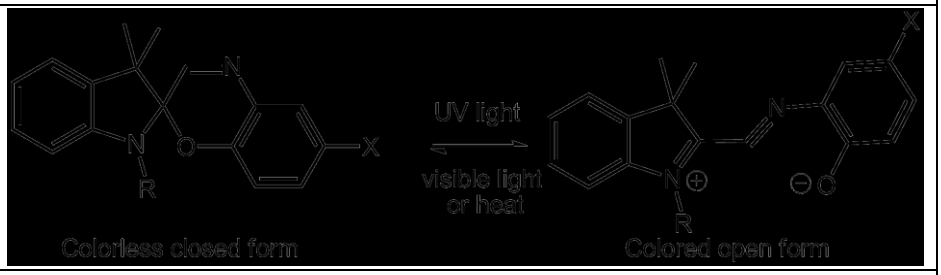
Diarylethenes	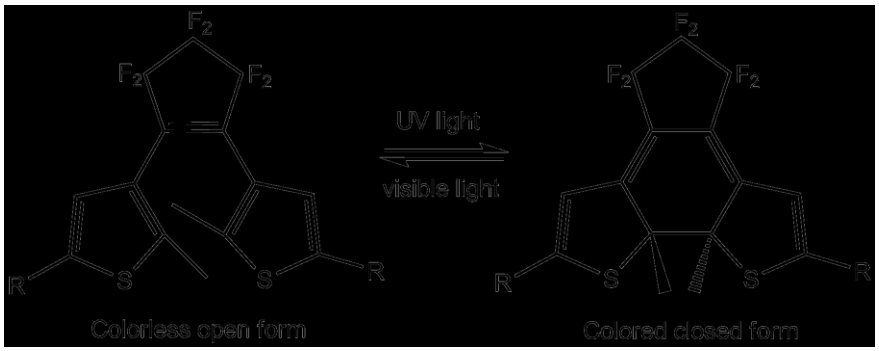
Azobezenes	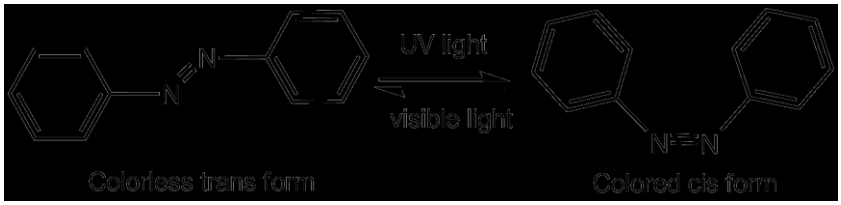

1.1.3. Spiropyrans and Their Properties

An important class of organic photochromes is the spiropyrans, owing to the dramatic changes in the optical properties upon irradiation with UV light. Spiropyran gets its name for the sp^3-hybridized "spiro" carbon in the pyran ring, which separates the two aromatic rings in the molecule (Figure 1.2). The two aromatic rings are perpendicular to each other. The spiropyran molecule has two isomers, the ring-closed spiropyran form

and the ring-opened merocyanine form. When irradiated with UV light, the “spiro” C-O bond in the pyran ring breaks and the pyran ring opens. The ‘spiro’ carbon becomes sp^2 hybridized with the adjacent nitrogen atom due to the lone-pair on the nitrogen. This configuration change leads the aromatic group rotating to align its π-orbitals with the rest of the molecule, forming a larger conjugated planar system. This new isomer is named merocyanine. Since the large conjugated system in merocyanine can absorb photons of visible light, the molecule appears colored. Spiropyrans are thermodynamically unstable in the ring-open form, the C-O bond gradually reforms in the dark at room temperature, the sp^2 carbon becomes sp^3 hybridized, and the colored merocyanine form reverts to the stable ring-closed colorless spiropyran form. Visible light irradiation accelerates the reverse process [1, 2, 3, 7].

1.1.4. Biological Applications of Spiropyrans

Traditionally, photochromic materials based on spiropyrans have been used as detectors [8], photochromic lenses for eye protection [9], and light filters with modulated transmission [10]. Spiropyrans also have been explored to use as molecular logic devices [11], photochromic and electro-optical devices [12], molecular and supramolecular logic switches [13], photoswitches [14], and multifunctional artificial receptors [15], molecular sensors [16-17], and optical data-recording devices [18], etc.

In recent years, spiropyrans have attracted a great deal of attention for biological applications. Andersson et al. showed that the ring-open form exhibited a strong affinity with DNA by intercalation, whereas the ring-closed spiropyran had little or no affinity for DNA. Thus, by photoswitching between the two forms, spiropyran can be used to modulate the behaviour of DNA [19]. In addition, a number of fluorophore-spiropyran

hybrid systems have also been recently reported in the literature and spiropyrans have also been hybridized with quantum dots (QDs) to modulate their fluorescence emission [20]. However, in most biological applications of spiropyrans, direct irradiation of UV light was used to trigger the isomerization transformation.

1.2. Lanthanide-Doped Upconversion Nanoparticles (Ln-UCNPs)

1.2.1. Spectroscopic Properties of Lanthanide ions

While some of the lanthanides may exist in the +2 and +4 oxidation states, the +3 oxidation state is the most prevalent and is generally known to be the most stable configuration for the lanthanide ions. A summary of the electronic configurations of the lanthanides and the trivalent ions is presented in Table 1.2.

Table 1.2: Electronic configurations of lanthanide atoms and trivalent ions [21-23]

Atomic Number	Element	Symbol	Electronic Configuration		Ln^{3+} Radius (pm)
			Atom	Ln^{3+}	
57	Lanthanum	La	$[Xe]6s^2 4f^0 5d^1$	$[Xe]4f^0$	103
58	Cerium	Ce	$[Xe]6s^2 4f^1 5d^1$	$[Xe]4f^1$	102
59	Praseodymium	Pr	$[Xe]6s^2 4f^3$	$[Xe]4f^2$	99
60	Neodynium	Nd	$[Xe]6s^2 4f^4$	$[Xe]4f^3$	98.3
61	Promethium	Pm	$[Xe]6s^2 4f^5$	$[Xe]4f^4$	97
62	Samarium	Sm	$[Xe]6s^2 4f^6$	$[Xe]4f^5$	95.8
63	Europium	Eu	$[Xe]6s^2 4f^7$	$[Xe]4f^6$	94.7
64	Gadolinium	Gd	$[Xe]6s^2 4f^7 5d^1$	$[Xe]4f^7$	93.8
65	Terbium	Tb	$[Xe]6s^2 4f^9$	$[Xe]4f^8$	92.1
66	Dysprosium	Dy	$[Xe]6s^2 4f^{10}$	$[Xe]4f^9$	91.2
67	Holmium	Ho	$[Xe]6s^2 4f^{11}$	$[Xe]4f^{10}$	90.1
68	Erbium	Er	$[Xe]6s^2 4f^{12}$	$[Xe]4f^{11}$	89
69	Thulium	Tm	$[Xe]6s^2 4f^{13}$	$[Xe]4f^{12}$	88
70	Ytterbium	Yb	$[Xe]6s^2 4f^{14}$	$[Xe]4f^{13}$	86.8
71	Lutetium	Lu	$[Xe]6s^2 4f^{14} 5d^1$	$[Xe]4f^{14}$	86.1

Detail spectroscopic studies of the lanthanide ions in the $LaCl_3$ host lattice were carried out by Gerhard H. Dieke and his co-workers in 1950's and 1960's. The observations and findings were presented in his book, "Spectra and Energy levels of Rare Earth Ions in Crystals" [24]. The Dieke Diagram (Figure 1.3) illustrates the energy levels

of the trivalent lanthanide ions ranging from 0 to 40,000cm^{-1}, and it is widely used by spectroscopists and researchers in various fields.

The lanthanide ions exhibit some unique spectroscopic properties when compared to other ions. The 4f electrons of the trivalent lanthanide ions show weak electron-phonon coupling and weak interactions with the surrounding environment, owing to the shielding of the completely filled sub-shells ($5s^2$ and $5p^6$). This results in the lanthanides showing narrow and sharp f-f transition peaks. Another important spectroscopic property of the lanthanides is the upconversion property. In the upconversion process, emission of higher energy photons is achieved through sequential absorption of multiple lower energy photons. This is because the lanthanides have more than one metastable 4f energy levels with the exception of Yb^{3+}, with typical lifetime in the range of 10^{-6}s - 10^{-2}s. The long lifetime 4f excited states which serve as an energy reservoir satisfy the basic requirement for the multi-photon absorption upconversion process. The long lifetime of metastable states is due to the low transition probabilities between the 4f excited states, since the f-f transitions are Laporte forbidden [25].

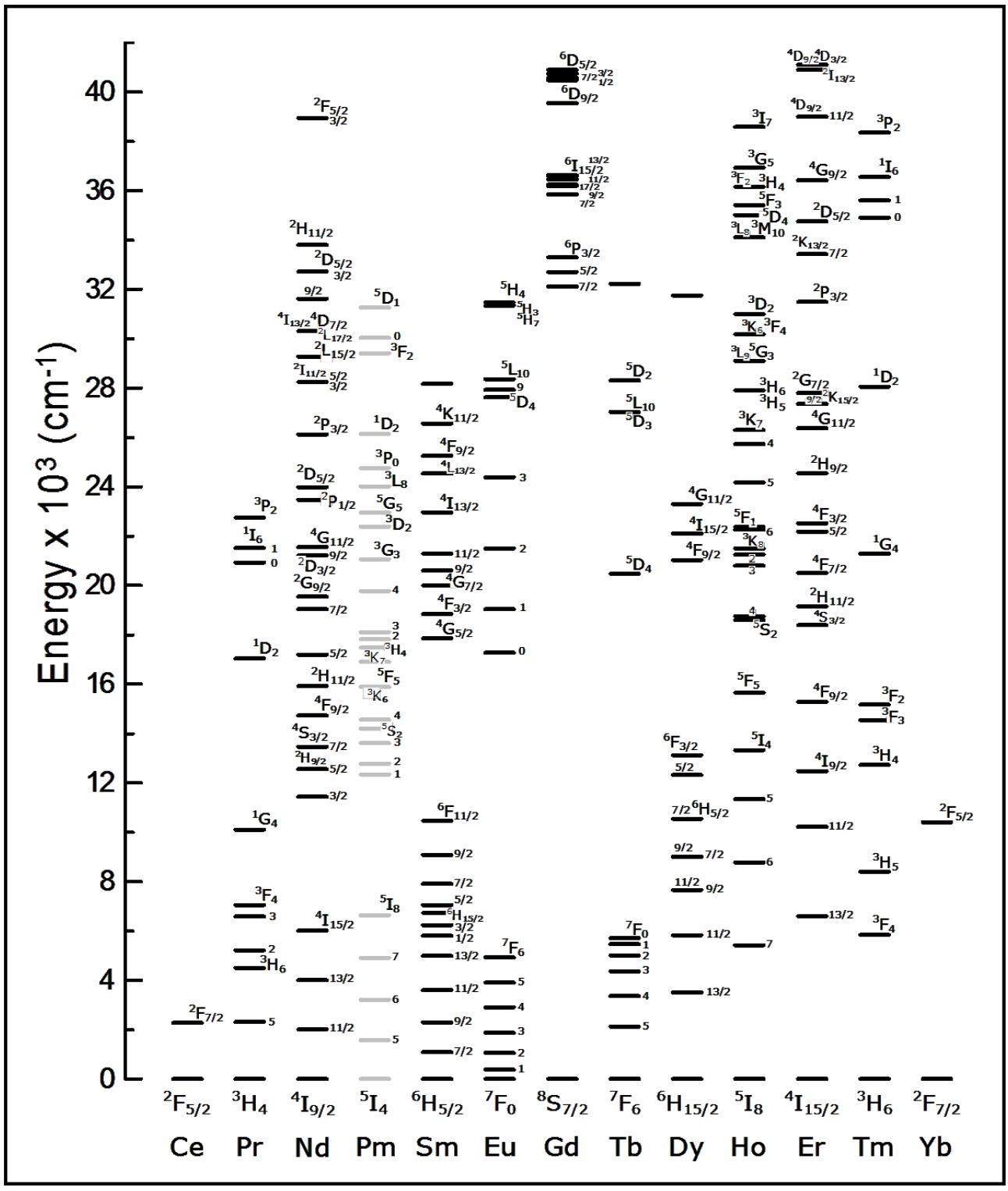

Figure 1. 3. Observed energy levels of the lanthanide ions in the $LaCl_3$ [25]

1.2.2. Upconversion Luminescence of Lanthanide-Doped Nanoparticles

The practical uses of the upconversion property of the lanthanides have mainly focused on bulk glasses and crystalline materials in the past thirty years, such as infrared quantum counter detectors, temperature sensors, and compact solid state lasers. Their usage was rarely found in biological science, due to the size restriction. With the emergence of nanoparticle research in the late 1990's, many synthetic methods were developed to prepare lanthanide-doped upconversion nanoparticles (Ln-UCNPs) with sizes in nanoscale region, high dispersibility and strong upconversion emission. Since then, lanthanide-doped upconversion nanoparticles attract large research interest in the interdisciplinary fields of photochemistry, biophysics, solid state physics, and materials science [26]. In particular, the upconversion emission of Ln-UCNPs offers an attractive optical labeling technique in biological assays and medical imaging, compared to conventional fluorophores such as organic fluorophores or quantum dots (QDs) [26].

Unlike organic fluorophores or QDs, which usually require UV excitation, Ln-UCNPs can be excited using lower energy light near infra-red (NIR) light to generate fluorescent emissions in shorter wavelength region (UV, visible). NIR excitation is superior to UV excitation in biological environment. Firstly, it can offer deeper penetration through tissues relative to UV sources. Surface tissues are mainly composed of hemoglobin, water, and lipids, which have their lowest absorption coefficient in the NIR region, so tissues can be highly penetrated. Secondly, NIR excitation causes less photo-damage to biological specimens (e.g., RNA, DNA) relative to UV. Lastly, NIR excitation significantly decreases auto-fluorescence from surrounding tissues compared to UV excitation [26-27].

In addition to using NIR excitation, another advantage of lanthanide-doped upconversion nanoparticles is the non-photobleaching, non-photoblinking and high spatial resolution in bioimaging. Lanthanide-doped upconversion nanoparticles have low-cytotoxicity to a broad range of cell lines. As a result, this property renders them a promising fluorescence imaging probe in biological application. Hence, Ln-UCNPs hold great potential as novel fluorophores for biological applications [26, 27].

Lanthanide-doped upconversion nanoparticles typically consist of an inorganic host lattice in which trivalent lanthanide dopant ions are doped. The lanthanide dopant ions function as the luminescent centers. In principle, upconversion can be expected in lanthanide-doped crystalline host materials; however, in order to obtain efficient upconversion lanthanide-doped nanoparticles, some selective criteria must be met. The most important aspects for preparing highly efficient upconversion lanthanide-doped nanoparticles are summarized below on the basis of long-term experimental experience [26-28].

1.2.2.1. Host Lattice

The host lattice is a transparent crystalline that accommodates the dopants. Good host lattice should satisfy the following criteria [26, 27]:

(i) close lattice matches to dopant ions;

(ii) low phonon vibration energies;

(iii) good chemical stability.

To meet the first standard, yttrium (Y) is commonly chosen as the cation in the host lattice, for Y^{3+} has very similar radius to the trivalent lanthanide ions (dopants); consequently, the dopant ions can easily substitute the Y^{3+} in the host lattice structure.

Among a wide variety of host lattices including oxides, bromides, chlorides, and fluorides, the latter are selected due to their low phonon energy and chemical stability. Low phonon energy decreases non-radiative multiphonon relaxation probabilities, thereby increasing the luminescence emission efficiency. So far, yttrium fluoride-based (i.e., $NaYF_4$) UCNPs have been identified as one of the most efficient upconversion luminescence nanoparticles.

Since the energy transfer upconversion (ETU) is more efficient than excited state absorption (ESA) in the multiphoton absorption upconvversion process, the energy transfer upconversion mechanism is widely applied in designing the lanthanide-doped upconversion nanoparticles. To enhance the luminescence efficiency of lanthanide-doped UCNPs in the energy transfer upconversion process, two types of dopant ions are needed. One is called an activator which is an energy acceptor and emits short wavelength photons; while the other acts as the donor of energy and is called the sensitizer. The selection of these two types of dopant ions is subject to the characteristics of the lanthanide ions' energy levels.

1.2.2.2. Activator

As can be seen in the Dieke Diagram, lanthanide ions (usually trivalent ions Ln^{3+}) commonly have multiple 4f energy-levels (with exception of La^{3+}, Ce^{3+}, Yb^{3+}, and Lu^{3+}) shielded by fully-filled 5s and 5p sub-shells. Laporte-forbidden f-f transitions reduce transition probabilities between f energy levels, thus prolonging the lifetime of the excited 4f energy levels (metastable states). As a result, lanthanide ions are ideal for upconversion emission. In practice, in order to obtain significant upconversion emission intensity, the activator should have a similar energy difference between each excited level

and its lower-lying energy level to facilitate photon absorption and energy transfer in the upconversion process; another condition is that the energy gap between the adjacent 4f energy levels should be large enough to minimize non-radiative relaxation. Ho^{3+}, Er^{3+} and Tm^{3+} have been shown to be the most suitable activators due to their ladder-like arranged 4f energy levels and relatively large energy gaps among the various excited levels, other lanthanides such as Tb^{3+} , Pr^{3+} ,Dy^{3+} have also been used as activators. The schematic energy levels of the widely-used activators Er^{3+} and Tm^{3+} are illustrated in Figure 1.4 [26-28].

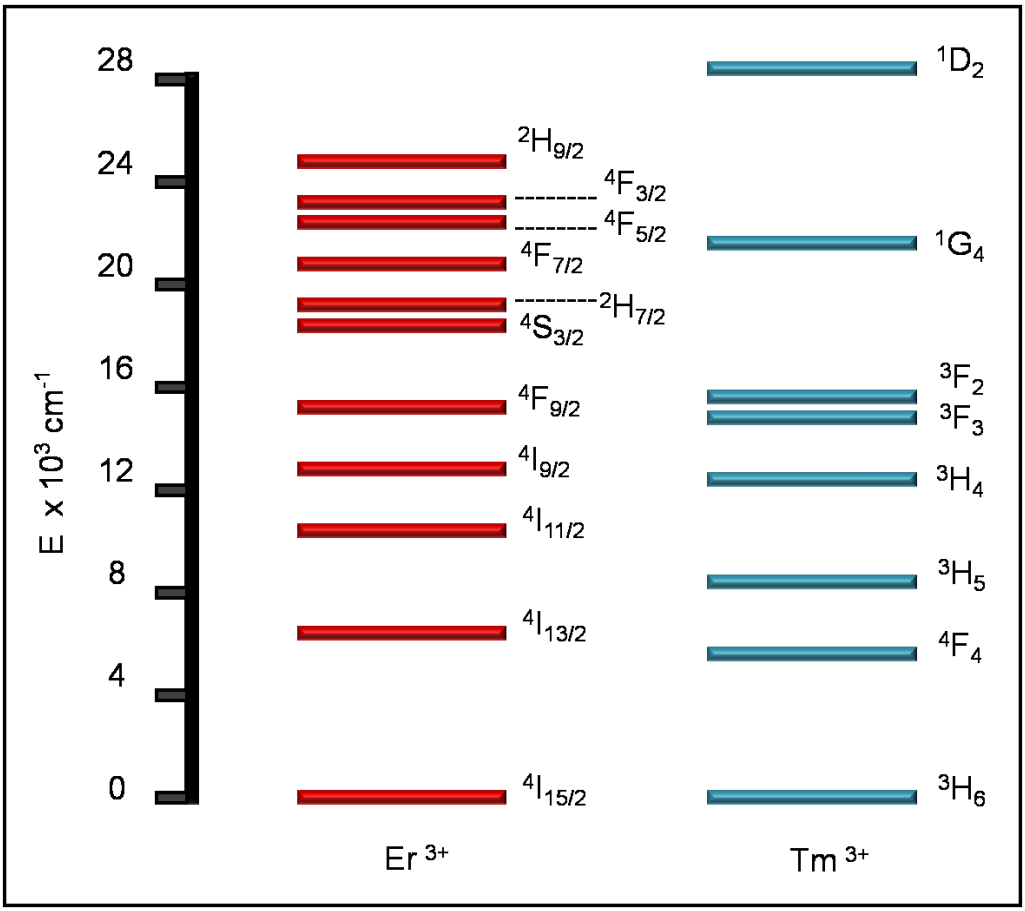

Figure 1. 4. Schematic energy level diagram for ions $Er^{3+}$and Tm^{3+}

1.2.2.3. Sensitizer

Although Er^{3+} and Tm^{3+} exhibit appropriate energy gaps, their low absorption cross-sections does not favour the absorption of photons, resulting in low upconversion luminescence efficiency. To improve upconversion luminescence efficiency, a sensitizer which has a higher absorption cross-section is co-doped with an activator in the host lattice. Taking advantage of the large absorption cross-section of the sensitizer, the pumping energy can be primarily absorbed by the sensitizer, and subsequently transferred to the activator via non-radiative energy transfer pathways, thus increasing the luminescence efficiency of the activator. In most studies, Yb^{3+} ion is selected as a sensitizer for several reasons:

(i) it has only one excited 4f energy level $^2F_{5/2}$ (Figure1.5), with an energy gap (between $^2F_{5/2}$ and $^2F_{7/2}$) resonant with the commonly-used 980 nm incident light;

(ii) its absorption band has a large absorption coefficient at this wavelength;

(iii) the energy difference between $^2F_{5/2}$ and $^2F_{7/2}$ is similar to those of the adjacent ladder-like arranged 4f energy levels in the activators such as Er^{3+} and Tm^{3+}, favouring the energy transfer from the sensitizer Yb^{3+} to activators Er^{3+} and Tm^{3+} [26-28].

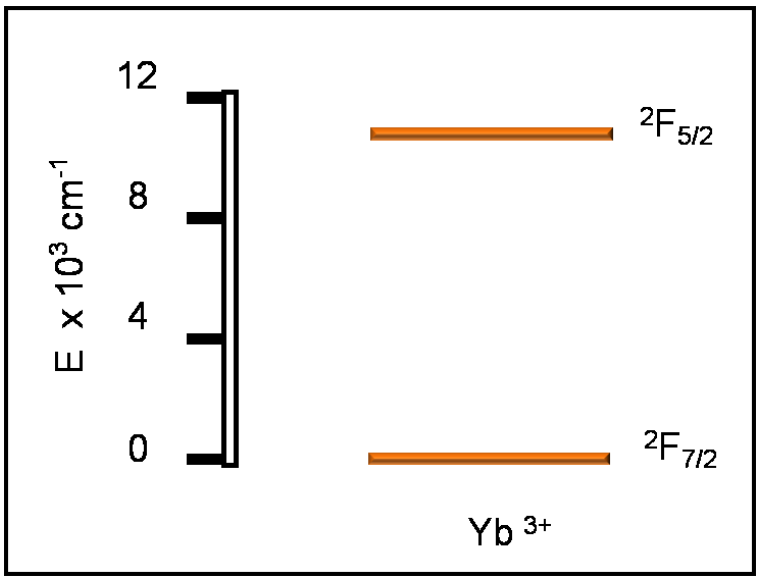

Figure 1. 5. Schematic energy–level diagram for ion Yb^{3+}

Besides selecting an appropriate host lattice and an appropriate activator and sensitizer, the relative concentration of the activator and sensitizer is extremely important in order to get highly-efficient upconversion nanoparticles. Typically, to minimize cross-relaxation energy loss, the concentration of the activator is relative low than 2 mol %, whereas, for the sensitizer, the concentration is relatively high (~20 mol %) [26].

1.2.3. Biological Optical Window and NIR-Excited Lanthanide-Doped UCNPs

Living organisms are composed of water and organic molecules. In particular, the surface tissues of organism consist mainly of water and organic molecules such as hemoglobin, oxygenized hemoglobin, and melanin. So the transparency of the surface tissues is dependent on the absorption abilities of these components in specific region. Typically, biological samples show a low absorption of radiation in the electromagnetic region between 600 to 1300 nm, known as biological optical window [29].

Lanthanide-doped upconversion nanoparticles are usually excited with NIR light (typically 980 nm) to generate emissions in the visible region. This excitation wavelength

falls in the biological optical window. Since NIR light has deep penetration and less scattering in biological samples, lanthanide-doped upconversion nanoparticles have been become promising optical labels *in vitro* and in vivo biological applications [26, 27].

1.2.4. $Tm^{3+/}Yb^{3+}$ Co-Doped $LiYF_4$ Upconversion Nanoparticles

Recent work carried out in our research group has shown that Tm^{3+}/Yb^{3+} co-doped $LiYF_4$ nanoparticles exhibited strong UV emissions at 353 and 368 nm (corresponding to transitions $^3P_0 \rightarrow {}^3F_4$ and $^1D_2 \rightarrow {}^3H_6$ respectively) via NIR (980 nm) excitation [30]. These strong upconversion UV emissions demonstrate that energy transfer between the activator ion Tm^{3+} and sensitizer ion Yb^{3+} in the $LiYF_4$ host lattice is efficient.

This phenomenon also suggests $LiYF_4$ is an efficient matrix for Ln^{3+} dopant ion (especially for Tm^{3+}) upconversion process at the nanoscale, because, to emit UV light, a sequential absorption of four and five pumping photons (980 nm) via energy transfer from ion Yb^{3+} to ion Tm^{3+} is required to populate the $^3P_0$ and $^1D_2$ excited states of the activator. The possible upconversion mechanism in the Tm^{3+}/Yb^{3+}co-doped $LiYF_4$ nanoparticles is shown in Figure 1.6 [30].

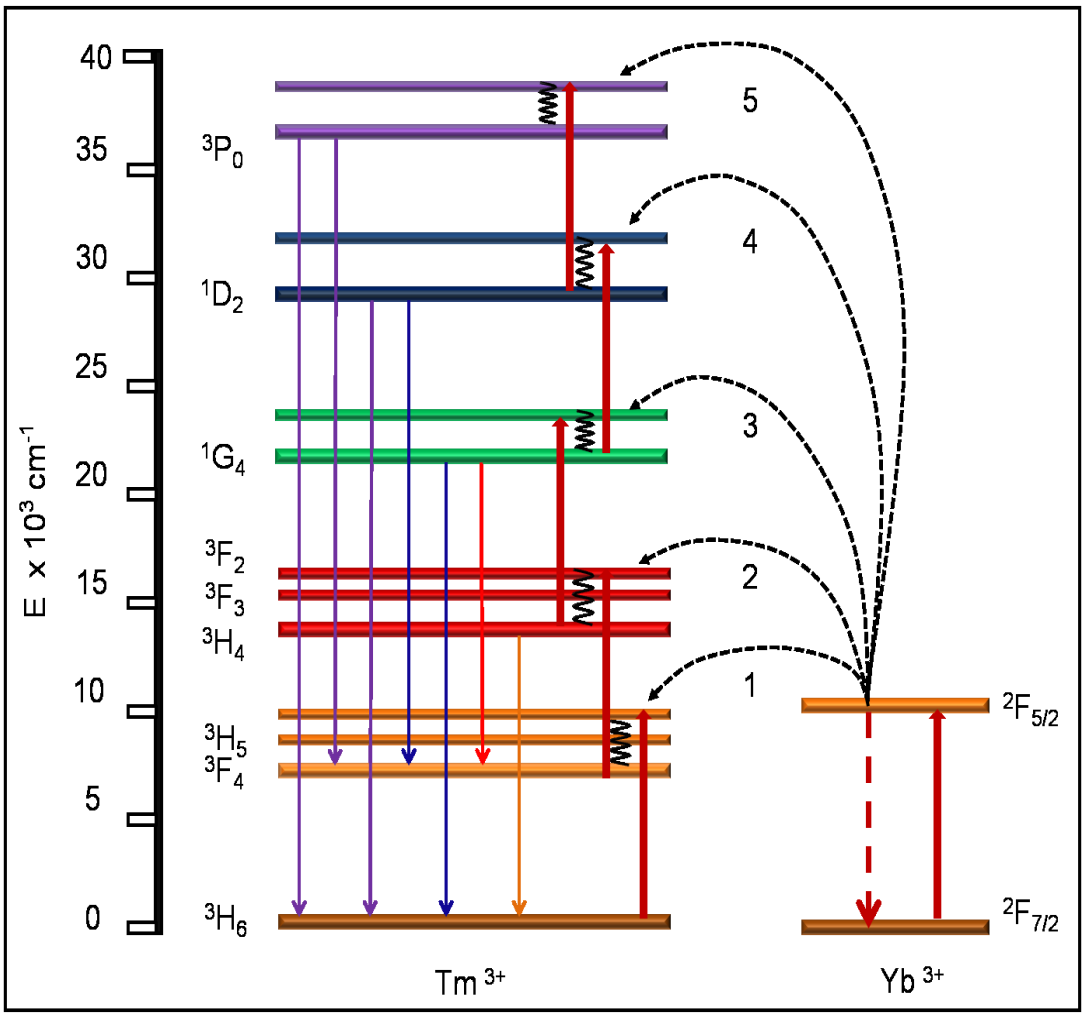

Figure 1. 6. Schematic representation of upconversion mechanism in Tm^{3+}/Yb^{3+} co-doped $LiYF_4$ nanoparticles

Due to the unique strong NIR-to-UV emission of Tm^{3+}/Yb^{3+} co-doped $LiYF_4$ nanoparticles, this type of UCNPs has the potential to function as an in-situ UV source for in vivo applications.

1.3. Objectives

1.3.1. Statement of The Problem

As mentioned before, photochromic compounds have been explored in biological applications in recent years. Applications of photochromic compounds such as spiropyrans require irradiation by UV light to trigger the isomerisation transformation. It is well established that excitation using UV light limits biological applications, because UV light has low tissue penetration depth due to its large scattering. Furthermore, UV light irradiation can lead to potential photodamage due to its high energy, and cause background autofluorescence in biological specimens [31].

1.3.2. Objectives

To avoid directly irradiating with high energy UV light in biological applications of spiropyrans, by incorporating the Tm^{3+}/Yb^{3+} co-doped UCNPs with spiropyrans, we could take advantage of the NIR-to-UV emission of Tm^{3+}/Yb^{3+} co-doped UCNPs to trigger the ring-opening transformation of spiropyran.

This thesis focuses on integrating the photochromic spiropyrans with Tm^{3+}/Yb^{3+} co-doped $LiYF_4$ nanoparticles to obtain a photoswitching model system for *in vivo* biological applications, as well as characterizing this new system.

To build this model system, we require a molecule, which not only contains the photochromic moiety, but also can be grafted to the surface of the UCNPs. For this purpose, bis-spiropyran(BSP) was synthesized as shown in Figure 1.7. This molecule contains two photochromic moieties and two carboxylic acid groups which can be used for functionalization to the surface of the UCNPs.

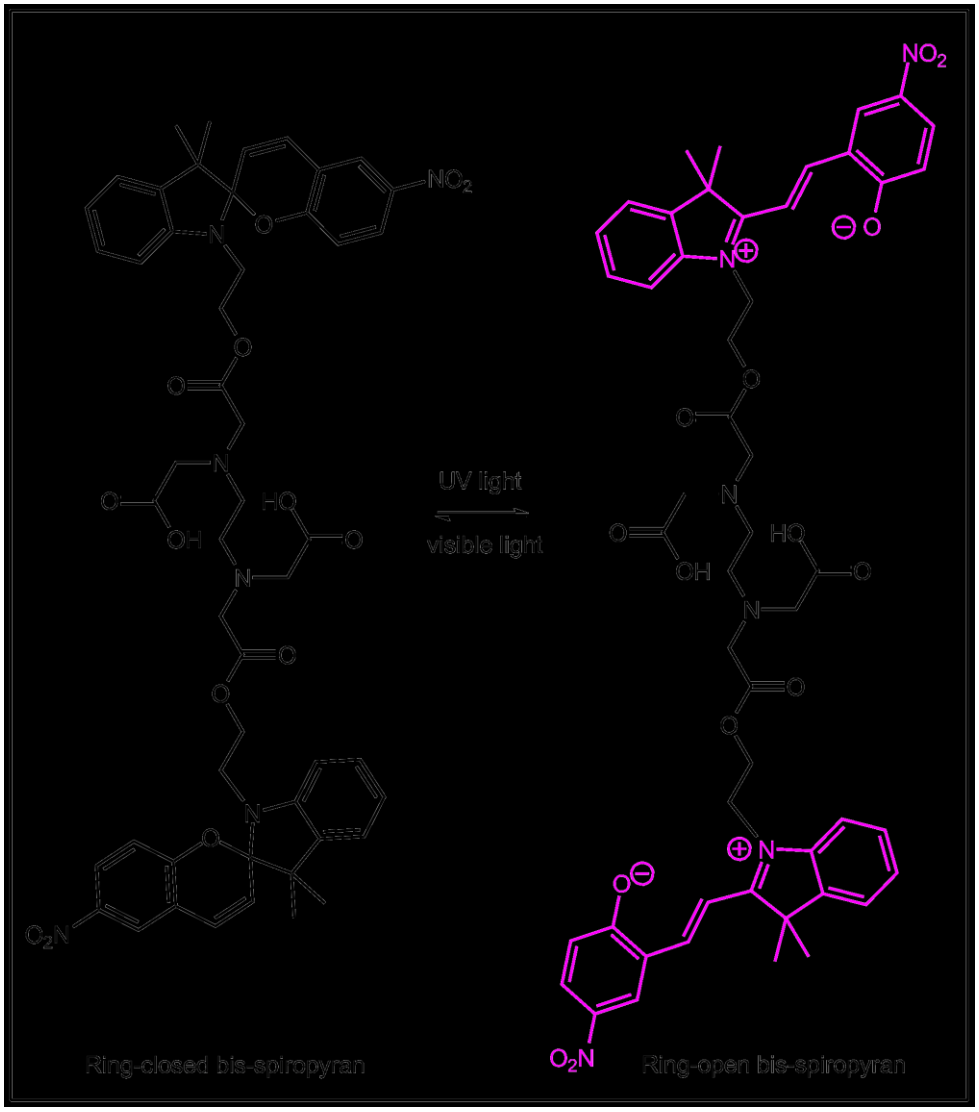

Figure 1. 7. Schemetic representation of photo-induced transformation between ring-closed bis-sipropyran and ring-open bis-merocyanine

The expected model system is illustrated in Figure 1.8. Bis-spyropyran molecules may be grafted on the surface of the UCNP by replacing the oleates which are capping the UCNPs, using a ligand-exchange process. Under irradiation by a 980 nm laser, the UV emission of the UCNPs generated through a multiphoton upconversion process will promote the isomerisation of ring-closed bis-spiropyran to ring-open bis-merocyanine with the aid of non-radiative fluorescence resonance energy transfer (FRET).

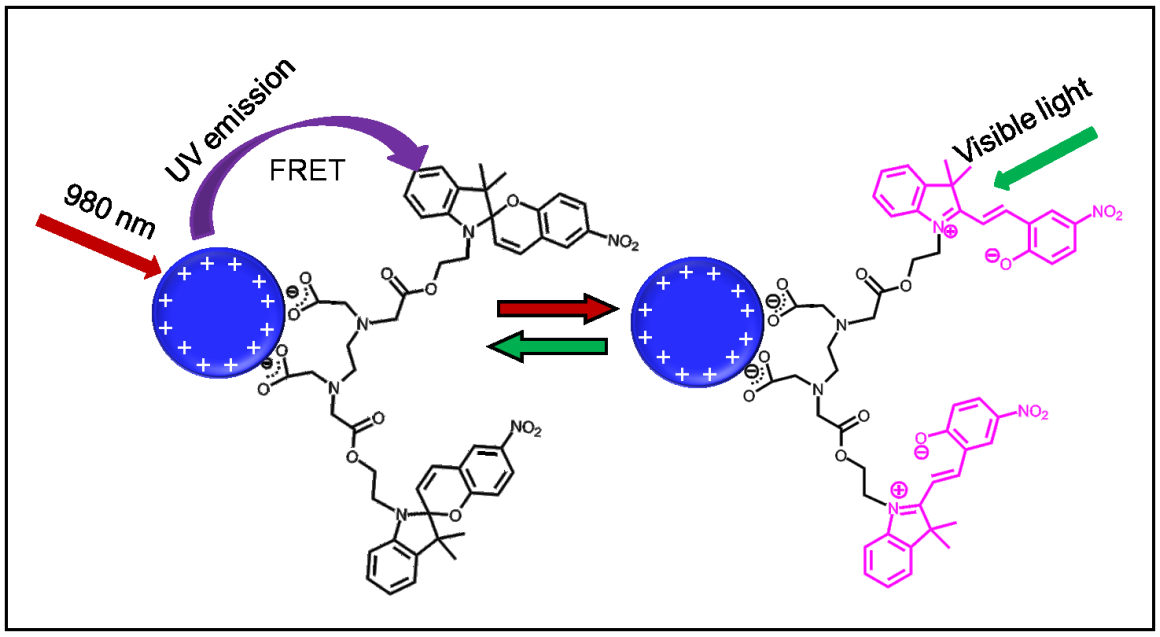

Figure 1. 8. Schematic of the BSP-UCNPs photoswitching system

After generating the model system, we will investigate the energy transfer efficiency between the UCNPs and the capping photochromic bis-spiropyran molecule under NIR irradiation to better understand the fluorescence resonance energy transfer process (FRET) in this model system.

The kinetics of the isomerisation under NIR irradiation, as well as the photo-degradation of bis-spiropyran, will be exploring to evaluate the feasibility of this system for in-vivo biological applications.

The knowledge acquired from these initial studies will be used in designing new NIR-triggered photoswitching systems suitable for in vivo biological applications such as drug delivery.

Chapter Two - Theory

2.1. Photochromic Mechanism of Spiropyran

Figure 2.1 shows the structure of a spiropyran molecule. The indoline moiety (left) and 2H-benzopyran moiety (right) are connected by the only common tertiary carbon atom, which forms two polar covalent bonds with the nitrogen of the indoline and the oxygen of the benzopyran respectively. The nature, electronic state, and relative orientation of the heteroatoms of the spiro centre affect the efficiency of n–σ* interactions (negative hyperconjugation) [32], thus changing the bond length between the heteroatoms and spiro carbon. The relative strength of theses interactions dictates which bond will break first, thus playing an important role in the photochemical activity of spiropyran family.

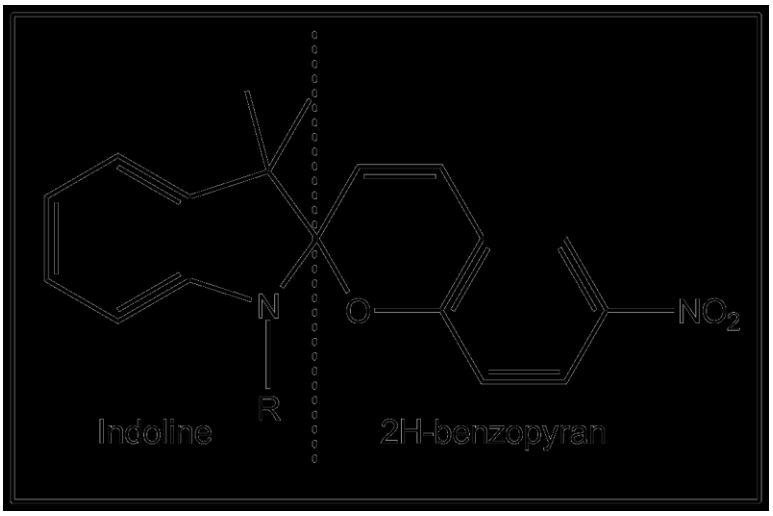

Figure 2.1. Schematic representation of spiropyran.

Before analyzing the relative strength of the n–σ* interactions, it is necessary to discuss the relative energy levels of the relevant orbitals. The electronegativity of the oxygen is greater than that of the nitrogen; therefore, the energy level of the electron pair

in the non-bonding orbital of the oxygen atom is lower than the energy level of the non-bonding orbital of the nitrogen atom. Similarly, the antibonding orbital σ*C-O is lower in energy than that of the σ*C-N. The relative energy levels of these four orbitals are shown in Figure 2.2.

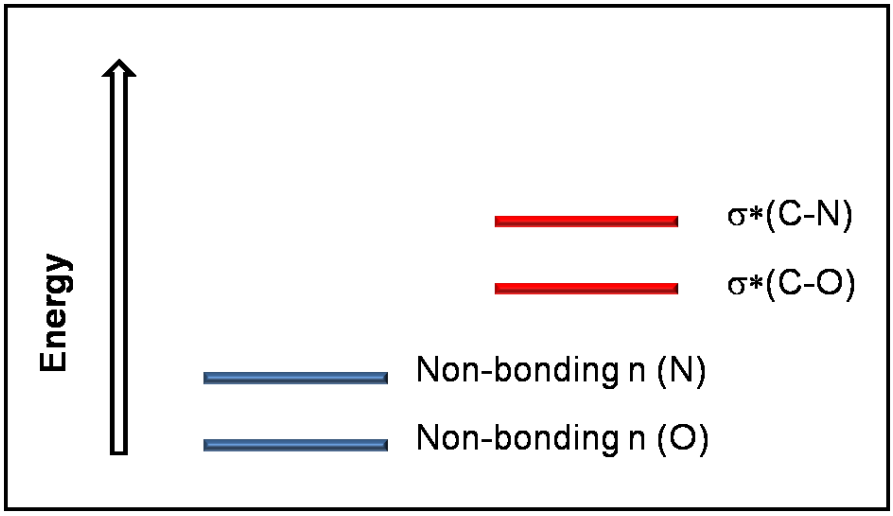

Figure 2.2. Relative energy levels of orbitals involved in negative hyperconjugation in spiropyrans.

In the ring-closed spiropyran conformation, the nitrogen orbitals have a pyramidal structure (Figure 2.3). The orbital (the apex) occupied by the lone electron pair is perpendicular to the base plane of the pyramid, and forming an obtuse angle with the aromatic plane of the indoline moiety with respect to the benzene ring. This orientation increases the distance between the π orbital of the benzene ring and the lone electron pair of the nitrogen, thus reducing the conjugation between them [33]. On the other hand, in this orientation, the lone-pair orbital is closer to the σ*(C-O) orbital, which promotes the donation of electron density from the lone-pair orbital to the empty antibonding σ*(C-O) orbital. This *n*–σ* interaction strengthens the C_{spiro}-N bond, while weakening the C_{spiro}-O bond [33].

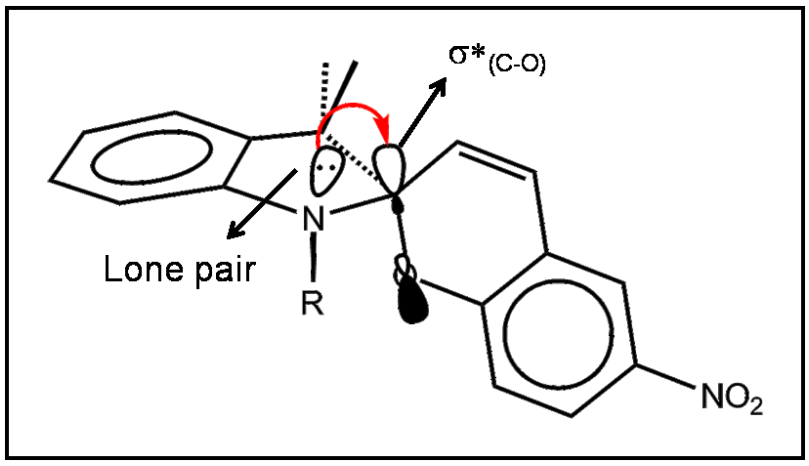

Figure 2.3. Schematic representation of the orientation of the lone electron pair of nitrogen atom and the anti orbital of σ*(C-O).

In the 2H-benzopyran moiety of spiropyran, the orbital of the lone pair electron of the oxygen occupies a *trans* position relative to that of the lone pair electron of the nitrogen, and it is perpendicular to the benzopyran aromatic plane. From the orientation of the lone pair orbital on the oxygen atom and the antibonding σ*(C-N) orbital depicted in Figure 2.4, similar *n*–σ* interaction is expected between the lone pair electron on the oxygen and the antibonding orbital σ*(C-N) [33].

Figure 2.2 shows that the energy difference between the non-bonding orbital of nitrogen and the antibonding σ*(C-O) orbital is smaller than that between the non-bonding orbital of oxygen and the antibonding σ*(C-N) orbital. Thus, the *n*–σ* interaction between the non-bonding orbital of nitrogen and the antibonding σ*(C-O) orbital should be stronger than that between the non-bonding orbital of oxygen and the antibonding σ*(C-N) orbital. Therefore, the electron density of the σ*(C-O) orbital is higher than that of the σ*(C-N) orbital. Overall, these *n*–σ* interactions lead to a strengthening of the C_{spiro}-N bond and a weakening of the C_{spiro}-O bond [33].

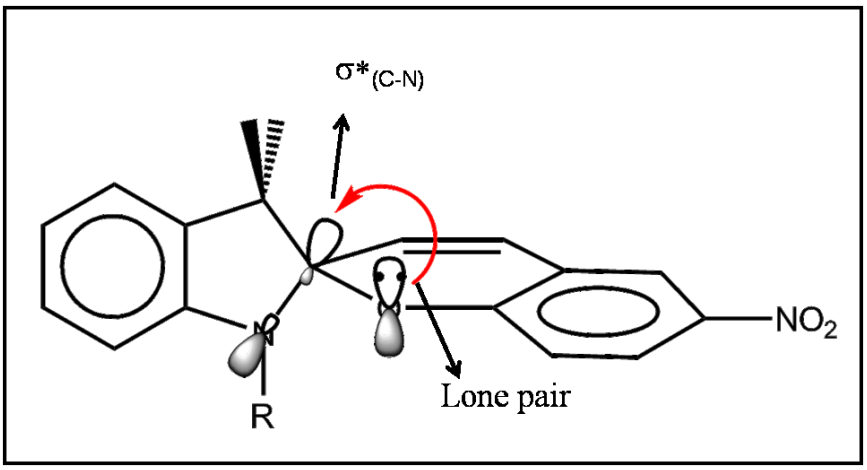

Figure 2.4. Schematic representation of the orientation of the lone electron pair of oxygen atom and the anti orbital of σ*(C-N).

It has also been shown that the photochromic activity of spiropyrans depends on the bond-length of the C_{spiro}-O**.** In general, Spiropyrans with a C_{spiro}-O bond length longer than 1.42 Å undergo photochromism; whereas those with C_{spiro}-O bond shorter than 1.42 Å do not [34].

Electron-withdrawing groups on the benzene ring linked to the pyran cycle have been shown to enhance the photochromic property of the spiropyran molecules. This results in the lengthening of the C_{spiro}-O bond via electron delocalization. For example, in spiropyrans with a para-nitro group (NO_2) on the benzene ring in the 2H-benzopyran moiety, the electron-withdrawing substituent can accept electron from the electron-rich benzene ring, leading to charge transfer from the lone pair electrons of the O to the π system of the benzene ring. Thus, this electron redistribution further weakens the C_{spiro}-O bond [3, 33, 35].

The last factor, which also plays an important role in the photochromic activity of spiropyrans is the degree of interaction between the indoline and the benzopyran moieties. We will discuss it in the section 2.2.

UV light excitation of spiropyran induces the cleavage of the elongated Cspiro-O bond, generating a relatively stable isomer (merocyanine, or MC form) via structural rearrangement (Figure 2.5). This change in structure leads to changes in the physical and chemical properties of the molecule, especially its color change in solution [3]. In this section, we will focus on the mechanistic pathway of this transformation.

Upon UV excitation, the Cspiro-O bond is cleaved, leading to the formation of cisoid intermediates (Figure 2.5 B) in a time scale of femtoseconds. These cisoid intermediates are higher in energy and unstable due to steric hindrance, since the two moieties of the molecule are still orthogonal to each other. Subsequent rotation of moieties of the molecule (with a time constant of picoseconds) leads to the formation of the more stable, transoid intermediates (Figure 2.5 C) since in this configuration non-bonding interactions in the molecule are minimized [3, 36]. The NO_2 on the benzene ring of spiropyran provides stabilization of the open merocyanine MC form since it enhances the delocalization of the negative charge on the oxygen as we discussed previously. In fact, the stable merocyanine form exists in two forms: a covalent quinone form and a zwitterionic form. The equilibrium between the two forms is dependent on the medium. Thus, the merocyanine MC isomer can be described as a resonance hybrid between a dipolar zwitterionic (Figure 2.5 D) and a quinonic form (Figure 2.5 E) [38].

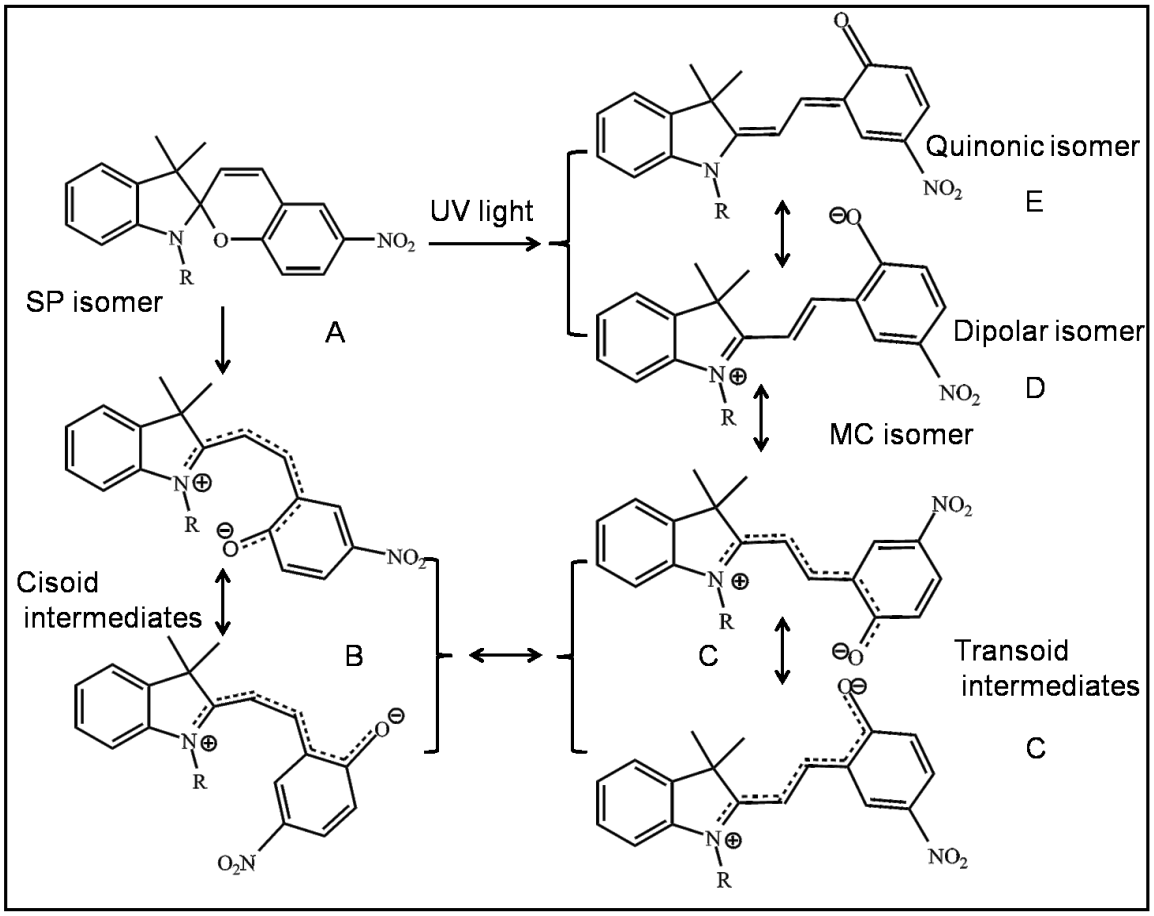

Figure 2.5. Schematic representation of the ring opening reaction under UV light irradiation and the pathway shown with the main intermediates and isomers

When the UV source is removed, the carbon-oxygen bond in the merocyanine isomer reforms, and the sp^2 hybridized carbon atom reverts to an sp^3 hybridization. The merocyanine MC isomer reverts back to ring-closed spiropyran isomer, which is colorless [3].

Figure 2.6 shows the relative energy of the isomers and the intermediates. It has been shown that the spiropyran SP isomer is thermodynamically stable with respect to the merocyanine isomer. The MC-to-SP transformation at room temperature [39] has been shown to follow first order kinetics, and heating or irradiating with visible light can accelerate the decoloration process [3].

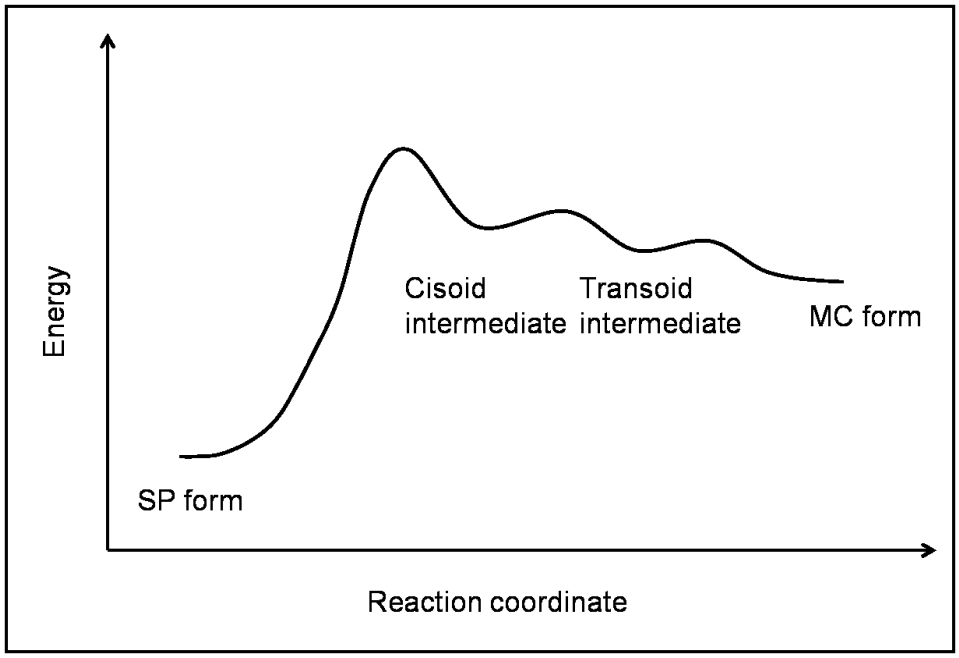

Figure 2.6. Energy diagram showing the pathway of the ring opening of spiropyran under UV light irradiation.

2.2. Spiro-Conjugation and Absorption Spectrum of Spiropyran

Spiro-conjugation is a characteristic π orbital overlap existing in some spiro-compounds, which exhibits a significant effect on their absorption spectra [40]. Generally speaking, a spiro-compound is a collection of molecules with two ring systems linked by the common spiro carbon atom (sp^3-hybridized). The two rings could function either as electron-donors or electron-acceptors, based on their structures (Figure 2.7) [41, 42].

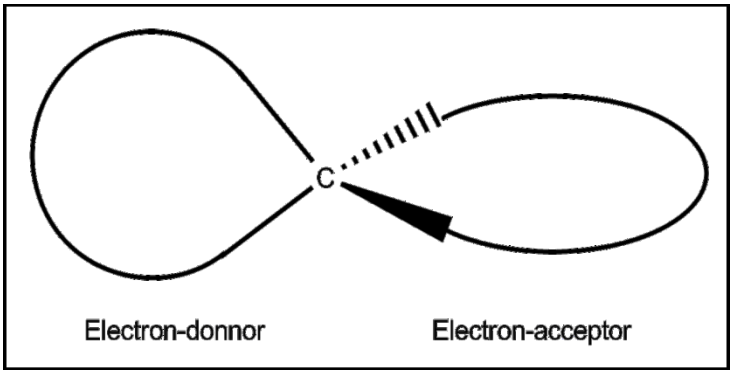

Figure 2.7. Schematic representation of spiro-compounds.

Conjugation between the two ring systems could occur, depending on the symmetry of the frontier orbitals of both ring systems. The frontier orbital of the electron-donor ring is HOMO while for electron-acceptor ring, the frontier orbital is HUMO. If the two frontier orbitals are both antisymmetric with respect to the two planes generated by the two rings of the molecule (Figure2.8 A and C), the corresponding frontier orbital presentations would be as shown in Figure 2.8 C and D. Obviously, a strong overlap occurs between them as shown in Figure 2.8 D. This overlap leads to the formation of a more stable orbital, resulting in the redistribution of the electrons in the molecule [41, 42]. This phenomenon is referred as spiro-conjugation, which leads to the appearance of a characteristic band in the visible region of the spectrum. For any other symmetry combinations, spiro-conjugation is very weak [43].

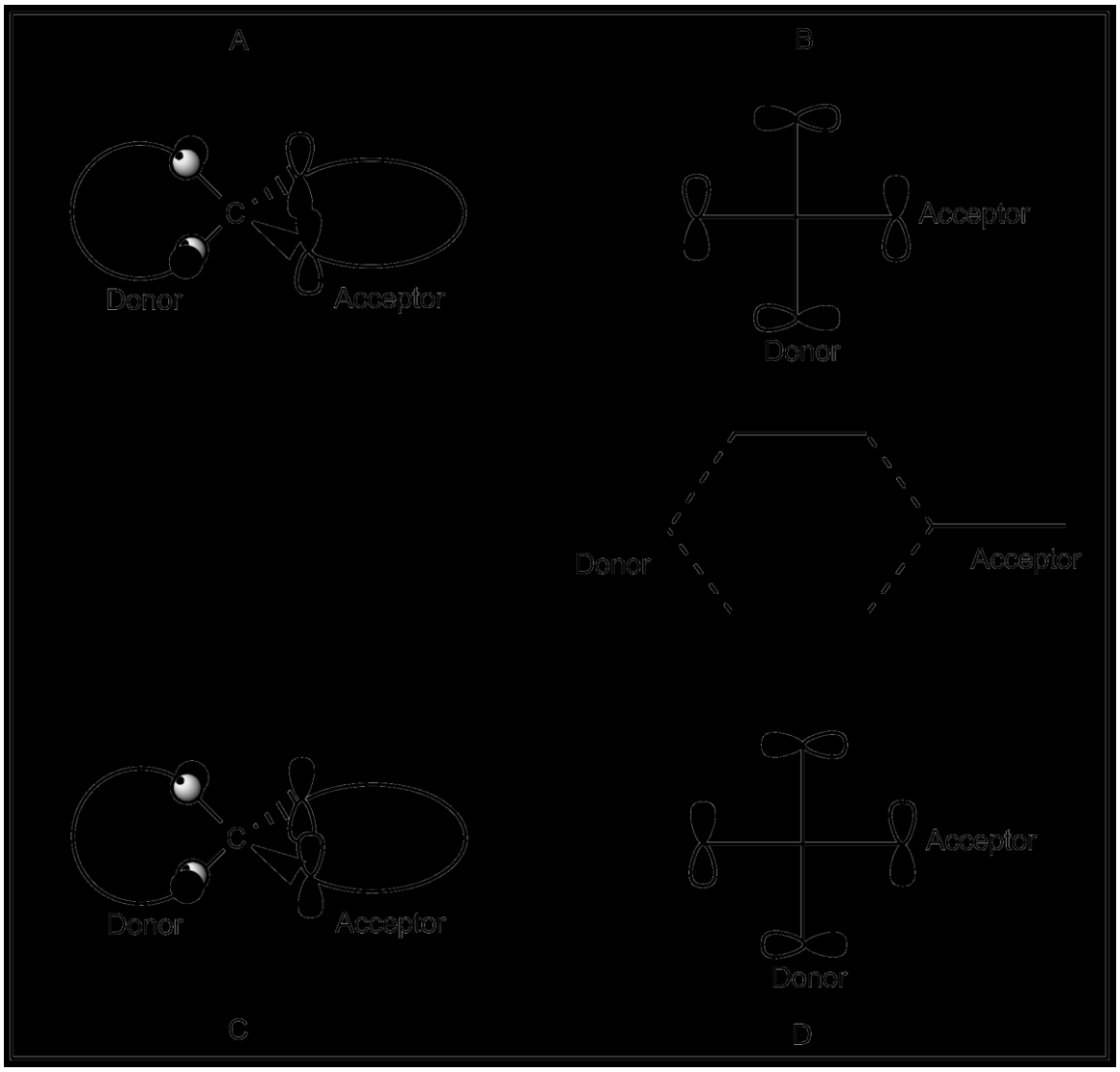

Figure 2.8. Scheme representing the frontier π orbitals in a spirocompound, whose two ring systems connected through a tetrahedral spiro carbon center. (A) and (C): Two cases showing the HOMO of the electron-donor and the LUMO of electron-acceptor are antisymmetric versus both molecular planes. (B) and (D): The corresponding symmetry representations of the π orbitals of the HOMO and the LUMO for both donor and acceptor.

Spiropyran consists of an indoline and 2H-benzopyran rings linked through a tetrahedral sp^3 carbon atom (Figure 2.9). The indoline moiety is an electron-donor, and its frontier orbital (HOMO) is symmetric; while the 2H-benzopyran moiety is an electron-acceptor, and its frontier orbital (LUMO) is antisymmetric.

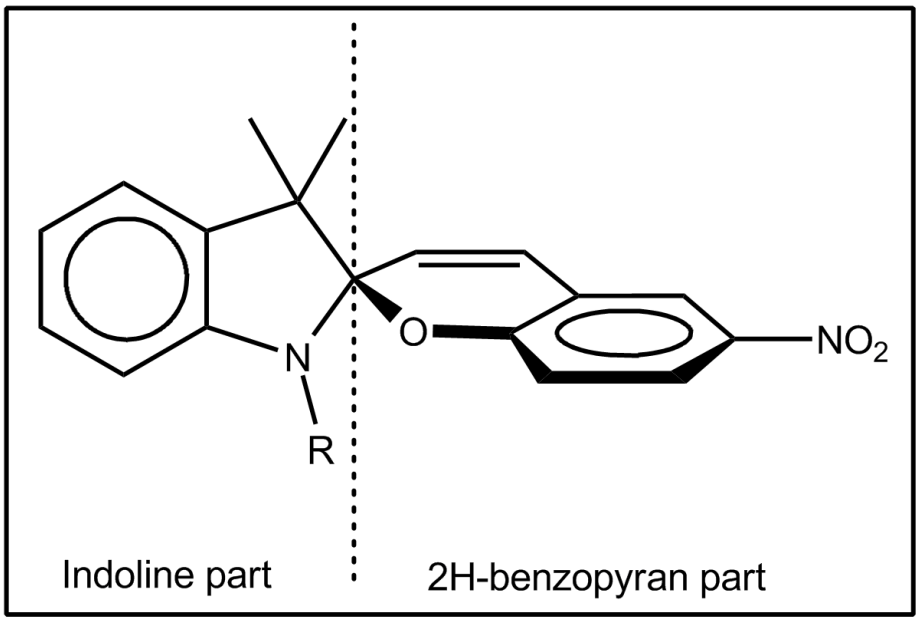

Figure 2.9. Schematic representation of the spiropyran showing the two perpendicular aromatic moieties- indoline and 2H-benzopyran parts.

Figure 2.10 A and C shows the two possible representations of the frontier π orbitals in spiropyran. In both cases, the two orthogonal π systems do not show strong interaction between the two moieties of the molecule based on their symmetry characters (Figure 2.10 C and D). Thus, weak or no spiro-conjugation exists in spiropyran. Therefore, absorption spectrum of the ring-closed spiropyran is simply the sum of the absorption spectra of the individual moieties with only a characteristic band between 200-400 nm [43].

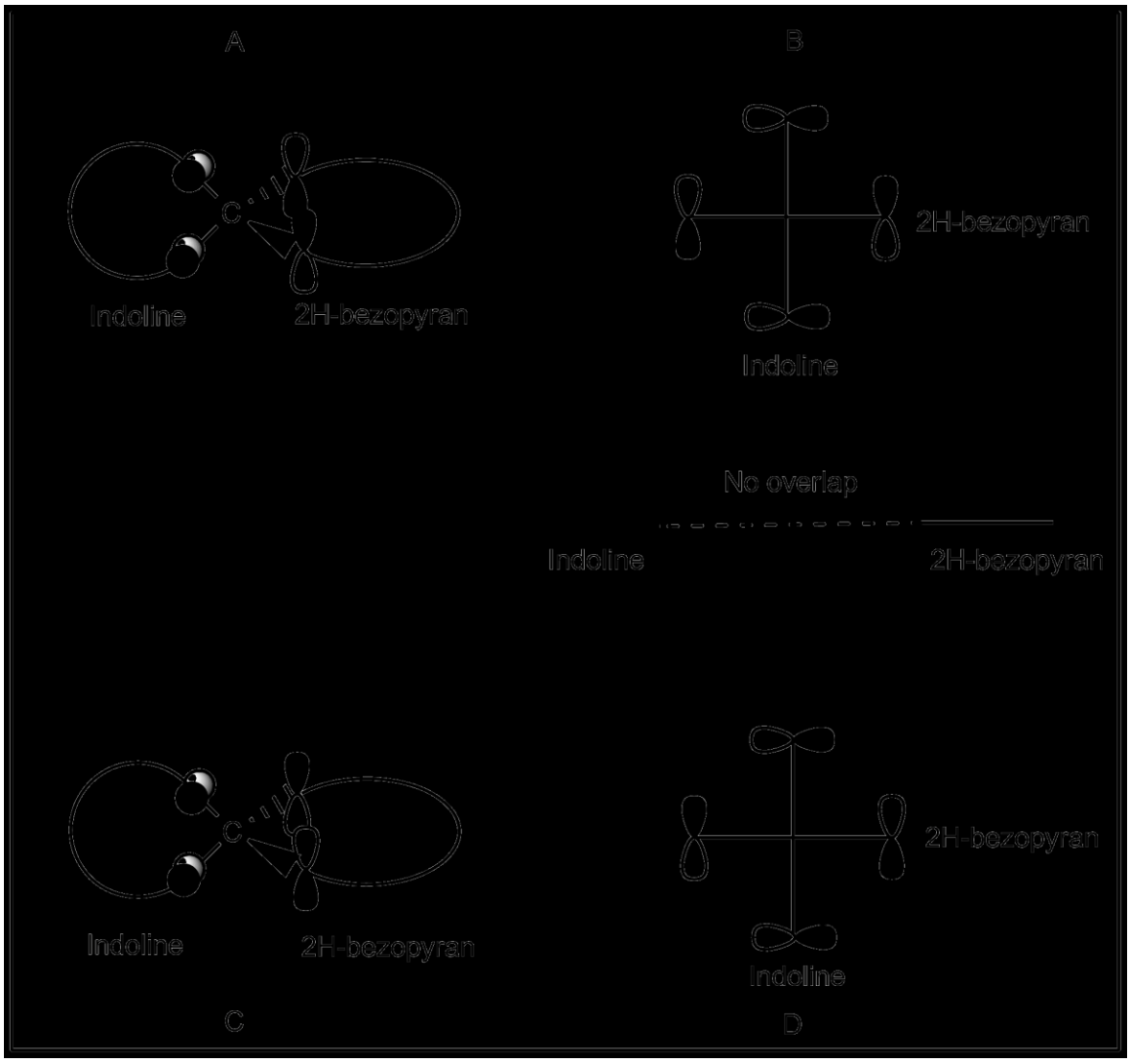

Figure 2.10. Scheme representing the frontier π orbitals in spiropyran. (A) and (C): Two cases showing the HOMO of the electron-donor is symmetric, and the LUMO of electron-acceptor is antisymmetric. (B) and (D): The corresponding symmetry representations of the frontier π orbitals of the HOMO and the LUMO for both donor and acceptor.

Upon UV irradiation, the C-O bond of the ring-closed spiropyran form is cleaved heterolytically, and the sp^3-hybridized spiro C acquires an sp^2 hybridization. The previously-isolated π electrons of aromatic rings in the molecule rotate and generate an extensively conjugated π system in the MC form (Figure 2.11). This extensive conjugated system can absorb light in the visible regions, usually between 500-600 nm [37].

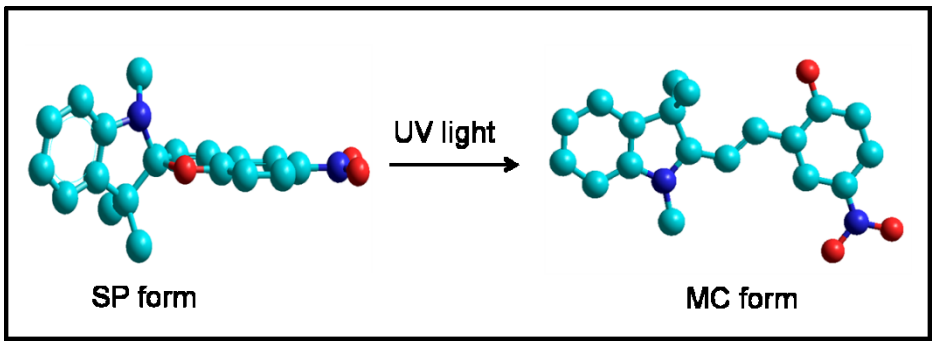

Figure 2.11. Ring-closed spiropyran SP form (left) with two orthogonal π systems is conversed into ring-open merocyanine MC form (right) with one enlarged planar conjugation π systems upon exposure to UV light.

2.3. Crystallization and Synthesis of Tm^{3+}/Yb^{3+} Co-Doped $LiYF_4$ Nanoparticles

Crystallization is a process of crystal formation in which solids precipitate from a solution, melt or gas. Supersatuation is the driving force for this process. Crystallization consists of two major events, nucleation and crystal growth. Initially, solute molecules in the solvent start to form nuclei; this process is called nucleation. Experimental conditions (temperature, supersatuation, etc) can affect the critical size of the nuclei, thus the crystal structure of a compound is dictated at the stage of nucleation. Subsequently, these nuclei serve as seeds and initiate the process of crystal growth in which more solute molecules deposit on the nuclei, following the same atom arrangement of the nuclei. Nucleation and crystal growth can occur simultaneously while the supersaturation exists. By adjusting the operating conditions, the rate of nucleation and crystal growth can be tuned to either nucleation or crystal growth predominant over the other. As a consequence, crystals with different sizes and shapes can be obtained [44, 45].

The synthesis of Tm^{3+}/Yb^{3+} co-doped $LiYF_4$ nanoparticles in my project was achieved via thermal decomposition, which in fact is a crystallization process of lanthanide trifluoroacetate precursors at high temperature. In order to preparing

appropriate UCNPs, the reaction conditions such as reaction temperature, time, and addition rate of precursor, have to be optimized [30, 46].

2.4. Upconversion

The simplest definition of upconversion is a process where low energy light such as NIR is converted to higher energy light such as UV, visible or even NIR (with a wavelength lower than the excitation source). Hence, following excitation, a system relaxes via the emission of photons of higher energy than those absorbed [25, 26, 47, 48].

Unlike simultaneous multi-photon processes, upconversion is a multiphoton process involving sequential absorption of at least two pump photons. One of the most important requirements is the presence of a metastable absorbing state which located between the ground and emitting states, acting as a population reservoir [25, 26].

There are three main types of mechanisms of the upconversion process: 1) excited state absorption; 2) energy transfer upconversion; and 3) photon avalanche [26]. The last of these was not observed in the work reported in this thesis and is therefore not discussed.

2.4.1. Excited State Absorption

Excited state absorption (ESA) process involves only a single ion, and the sequential absorption of two or more photons promotes the ion from the ground state to the excited state. This mechanism was first discussed by Bloembergen as the basis for an infrared quantum counter [49]. In Figure 2.12 below, ion X is in the ground state. An incoming pump photon of a wavelength resonant with the energy gap separating ground state G and excited state E_1 will promote the ion to this excited state. Since excited state E_1 has a long lifetime, a second incoming pump photon can promote the ion to a higher

excited state E_2 before it relaxes back to the ground state. Relaxation of the ion from the excited state E_2 to its ground state produces emission of photons with shorter wavelength than the pumping photon. Assuming the energy gap separating G and E_1 and E_1 and E_2 are equal, the same pump wavelength may be used; otherwise multiple-pumping sources are required [26].

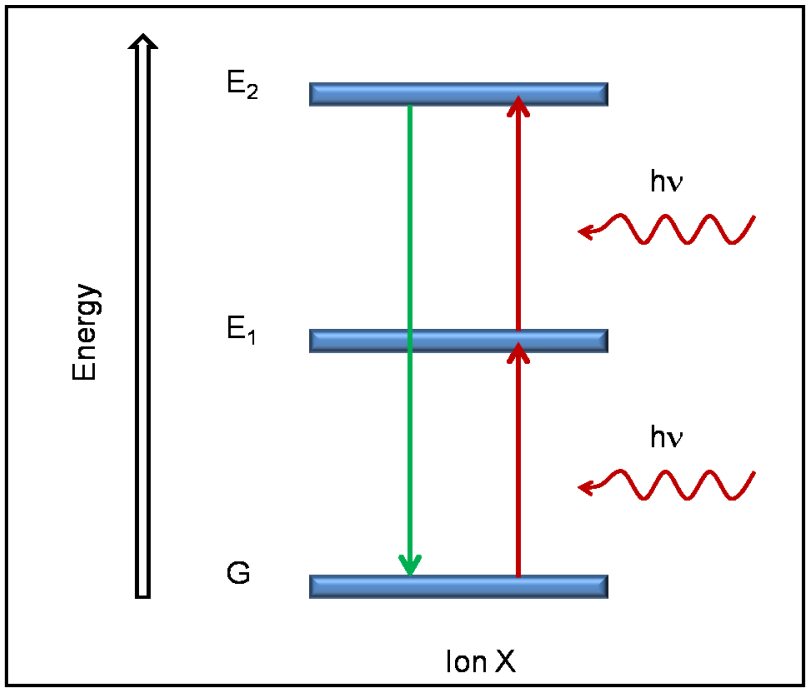

Figure 2.12. A general mechanism for excited state absorption (ESA) in a simple three energy level system.

2.4.2. Energy Transfer Upconversion

Energy transfer upconversion(ETU) was first observed and discussed by Auzel [25]. Most of the early studies on this mechanism were carried out on Er^{3+}/Yb^{3+} and Tm^{3+}/Yb^{3+} co-doped crystals in the mid 1960's [25, 48, 50]. ETU occurs via energy transfer between a neighbouring pair of ions where one acts as a donor, while the second as an acceptor of energy. A simplified mechanism of ETU is shown in Figure 2.13. An incoming pump photon, corresponding to the energy gap separating states G and E_1,

promotes both donor ions Y (usually an ion with a high absorption cross-section) to the intermediate excited state E_1. In the second step, a non-radiative energy transfer from the donor ion Y to the acceptor ion X results in the promotion of the latter to its excited state E_1 after which a second energy transfer promotes the acceptor ion to excited state E_2. Following the energy transfer, the donor ions Y relax to their ground state while the acceptor ion, now in E_2, undergoes a radiative decay with emission and returns to its ground state.

The upconversion efficiency in the ETU process is largely dependent on the overall concentration of dopant ions, because it determines the average distance between neighboring dopant ions in the lattice [25, 26].

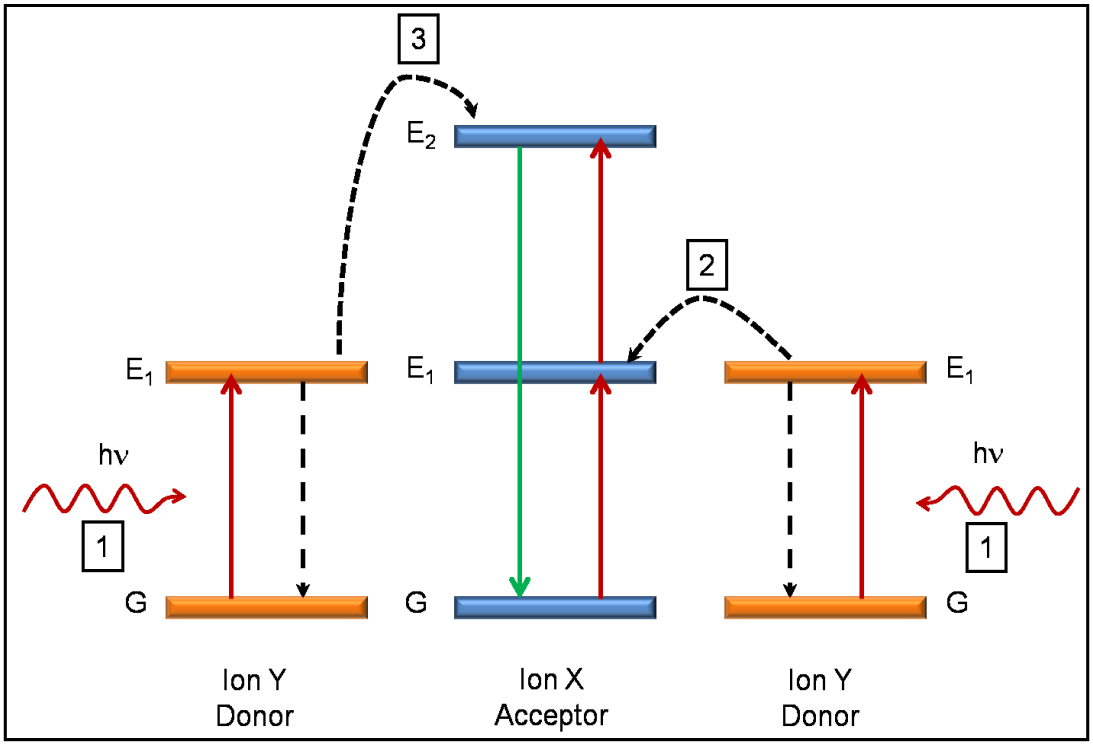

Figure 2.13. A general mechanism for energy transfer upconversion (ETU) in a simple three energy level system.

2.5. Förster Resonance Energy Transfer (FRET)

Förster resonance energy transfer (FRET) is a process by which an initially excited donor relaxes to the ground state by transferring its energy to a nearby acceptor in a non-radiative way (without the emission of a photon). The more common term Fluorescence Resonance Energy Transfer is also used for FRET to imply that the acceptor is a fluorophore. The theory of FRET has been developed for a long time and there are a number of reviews which have been written. The basic principle of FRET is shown in Figure 2.14. The donor initially absorbs energy and is excited to a high energy level. After relaxation, the fluorescence emission of donor is wholly or partially quenched by a radiationless energy transfer (FRET) to the acceptor, without conversion to thermal energy. The transfer of energy leads to a reduction in the donor's fluorescence intensity and its excited state lifetime, and excitation of the acceptor. As a result of the energy transfer to the acceptor, an emission from the acceptor is observed [51].

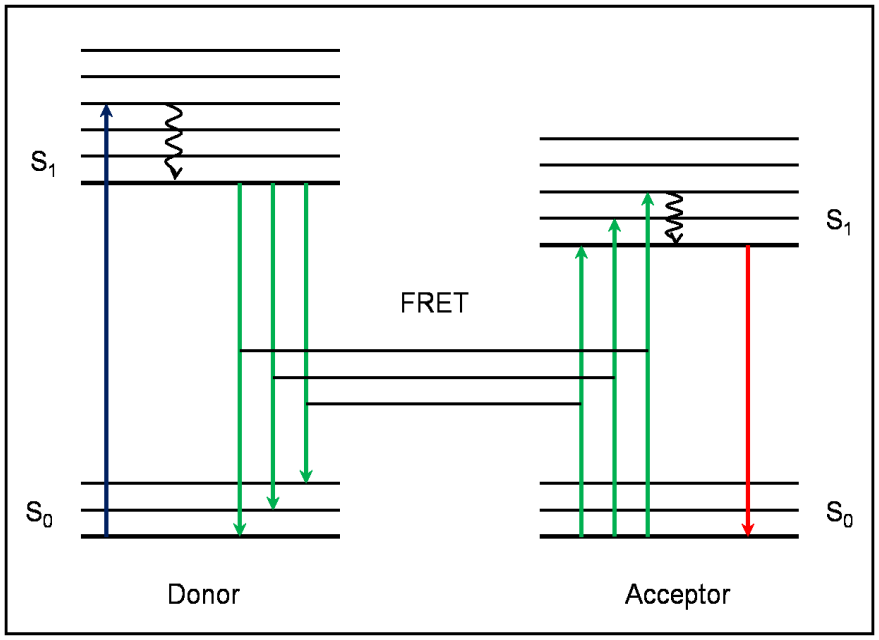

Figure 2.14. Jablonski diagram of fluorescence resonance energy transfer [51].

While there are many factors that influence FRET, our goal in this section is to simply emphasize the crucial parameters for the energy transfer efficiency, which are important to this thesis.

The first parameter is the distance (r) between the donor and acceptor. In the FRET process, the energy transfer efficiency is greatly dependant on the distance (r) between the donor and acceptor and Förster distance (R_o). Förster demonstrated that the efficiency of the process (E) depends on the inverse sixth power of the distance between donor and acceptor as shown in the following equation (1) [51].

$$E = \frac{R_0^6}{(R_0^6 + r^6)} \quad \ldots\ldots\ldots\ldots\ldots (2.1)$$

Where R_o is the Förster distance at which half the energy is transferred

and r is the actual distance between donor and acceptor.

Another important parameter is spectral overlap integral (Figure 2.15), the extent of spectral overlap between the donor emission and the acceptor absorption spectrum. It affects the Förster distance R_o.

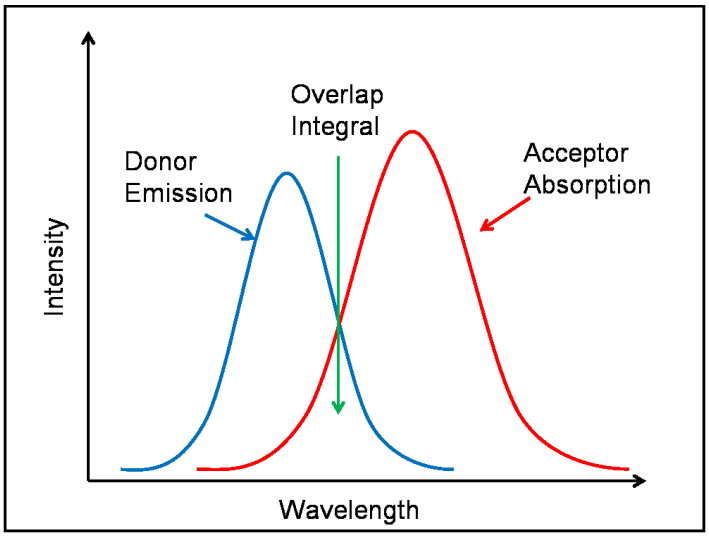

Figure 2.15. Schematic representation of the FRET spectra overlap integral [51].

The magnitude of the R_o is dependent on the spectral properties of the donor and the acceptor, as shown in Equation (2) [51].

$$Ro = 9.78 \times 10^3 \sqrt[6]{n^{-4} \times fd \times k^2 \times J}\ \text{Å} \ldots\ldots\ldots\ldots\ldots\ldots (2.2)$$

Where fd is the fluorescence quantum yield of the donor in the absence of acceptor

n is the refractive index of the solution

k^2 is the dipole angular orientation of each molecule

and J is the spectral overlap integral of the donor and acceptor.

Chapter Three

Photoswitching of Bis-Spiropyran Using Upconversion Luminescent Tm^{3+}/Yb^{3+}-Co-Doped Lithium Yttrium Fluoride Nanoparticles

Published as:

B. F. Zhang, M. Frigoli, F. Angiuli, F. Vetrone and J. A. Capobianco

Chem. Commun., 2012, **48**, 7244–7246

3.1. Abstract

Bis-spiropryran molecules were grafted onto the surface of upconverting nanoparticles. Fluorescence resonance energy transfer from the upconverting nanoparticles to the surface bis-spiropyran molecules triggered the transformation of the ring-closed bisspiropyran to the ring-open bis-merocyanine forms.

3.2. Introduction

Photochromism is defined as a light induced reversible interconversion of molecules between two states with a distinct absorption signature across the ultraviolet and visible regions of the electromagnetic spectrum [2, 52, 53]. The main families of organic photochromic compounds include spiropyrans, spirooxanines, diarylethenes, azobezenes, and fulgides [54]. These photochromic molecules are widely studied for their potential applications in molecular electronic and photonic devices [6, 16, 17, 55, 56]. In this context, one of the most widely studied organic photochromic families, spiropyrans, have attracted a great deal of attention for biological applications in recent years [57, 58]. The spiropyran molecule has two isomers, the ring-closed spiropyran form and the ring-opened merocyanine form. Irradiation of the colourless spiropyran form with UV-light not exceeding 450 nm produces the colored merocyanine form, which has a strong absorption in the visible and can be reversed by exposing it to yellow light. Upon UV irradiation, the C–O spiro bond is cleaved heterolytically and the spiro carbon, which is sp^3- hybridized becomes sp^2-hybridized producing a delocalized pi-system in the merocyanine form that is capable of absorbing light in the visible region.

Andersson et al. showed that the ring-open form exhibited a strong affinity with DNA by intercalation, whereas the ringclosed spiropyran had little or no affinity for

DNA.[19] Thus, by photoswitching between the two forms, spiropyran can be used to modulate the behaviour of DNA.[19] In addition, a number of fluorophore-spiropyran hybrid systems have also been recently reported in the literature and spiropyrans have also been hybridized with quantum dots (QDs) to modulate their fluorescence emission.[20]

However, for the biological applications of spiropyrans, direct irradiation with UV light was needed to trigger the isomerisation transformation. Excitation with high-energy UV light source obviously limits their use in biological applications due to its low tissue penetration depth, potential for photodamage and autofluorescence in biological specimens where chromophores are present [59].

Lanthanide-doped upconverting nanoparticles (UCNPs) have been intensively studied in recent years [26, 30, 60-66]. These nanoparticles can emit UV, visible and/or near-infrared (NIR) light upon NIR excitation (typically 980 nm) via a multiphoton process known as upconversion[25, 67-68]. Our group has recently synthesized Tm^{3+}/Yb^{3+} -doped $LiYF_4$ UCNPs via the thermal decomposition method, which showed stronger UV emission following NIR excitation with 980 nm light compared to $NaYF_4$ [30]. Taking advantage of the high penetration depth, reduced photodamage, and minimal autofluorescence of the NIR excitation light, these UCNPs could be used as biocompatible UV sources in biological applications. Incorporating spiropyrans with UCNPs could achieve the photochromic transformation of spiropyran upon NIR excitation through fluorescence resonance energy transfer (FRET) process.

In this communication we report on the functionalization of $LiYF_4:Tm^{3+}$, Yb^{3+} UCNPs with bis-spiropyran (Figure 3.1 and Figure 3.2) to demonstrate the

photoswitching of this molecule using the UV light obtained after NIR excitation of the nanoparticles. We also carry out a kinetic study of the photoswitching and report on the energy transfer efficiency between the UCNPs and the ring-closed bis-spiropyran as well as the photodegradation of the bis-spiropyran functionalized UCNPs (BSP-UCNPs).

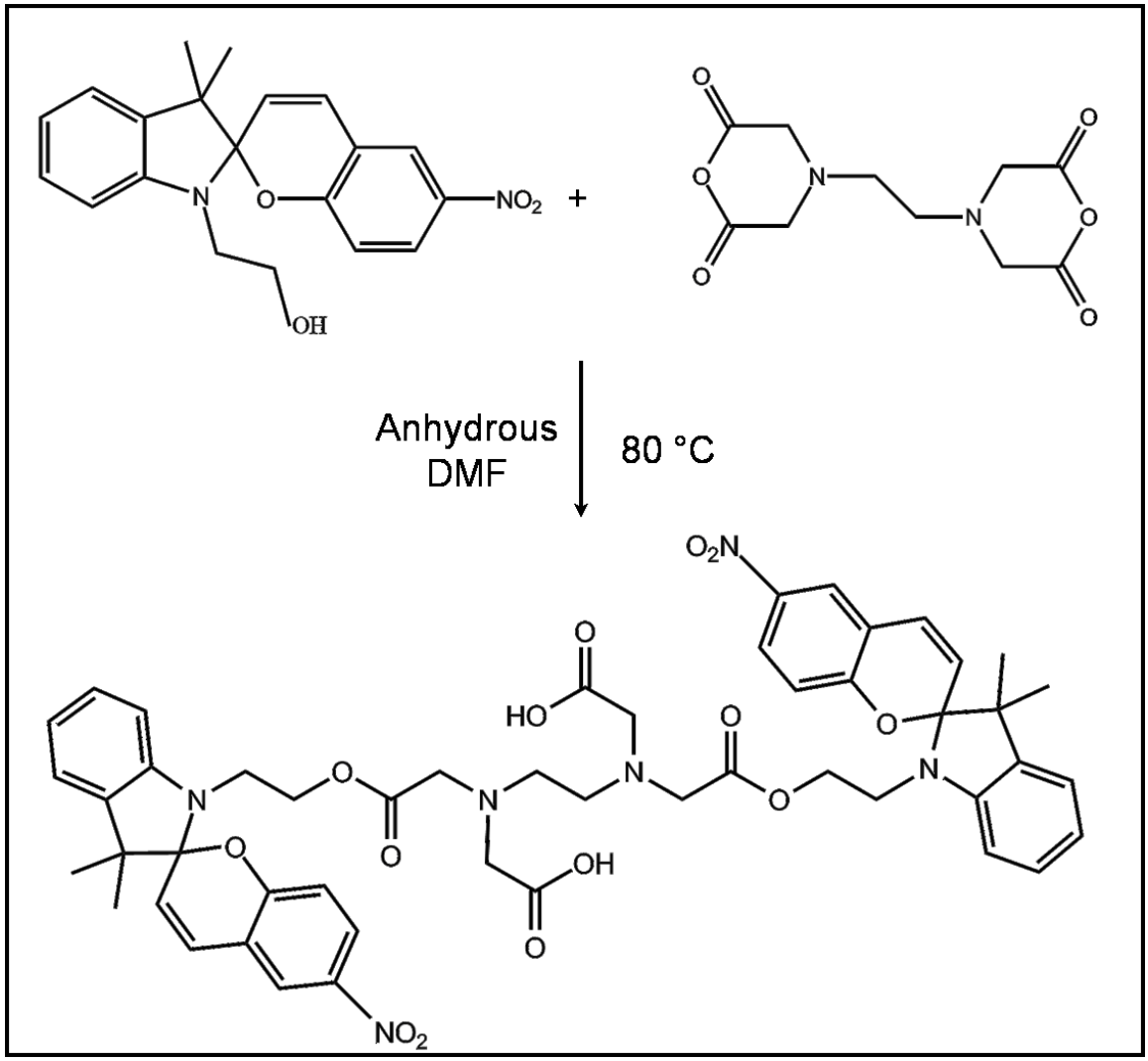

Figure 3.1: Reaction scheme used to prepare bis-spropyran.

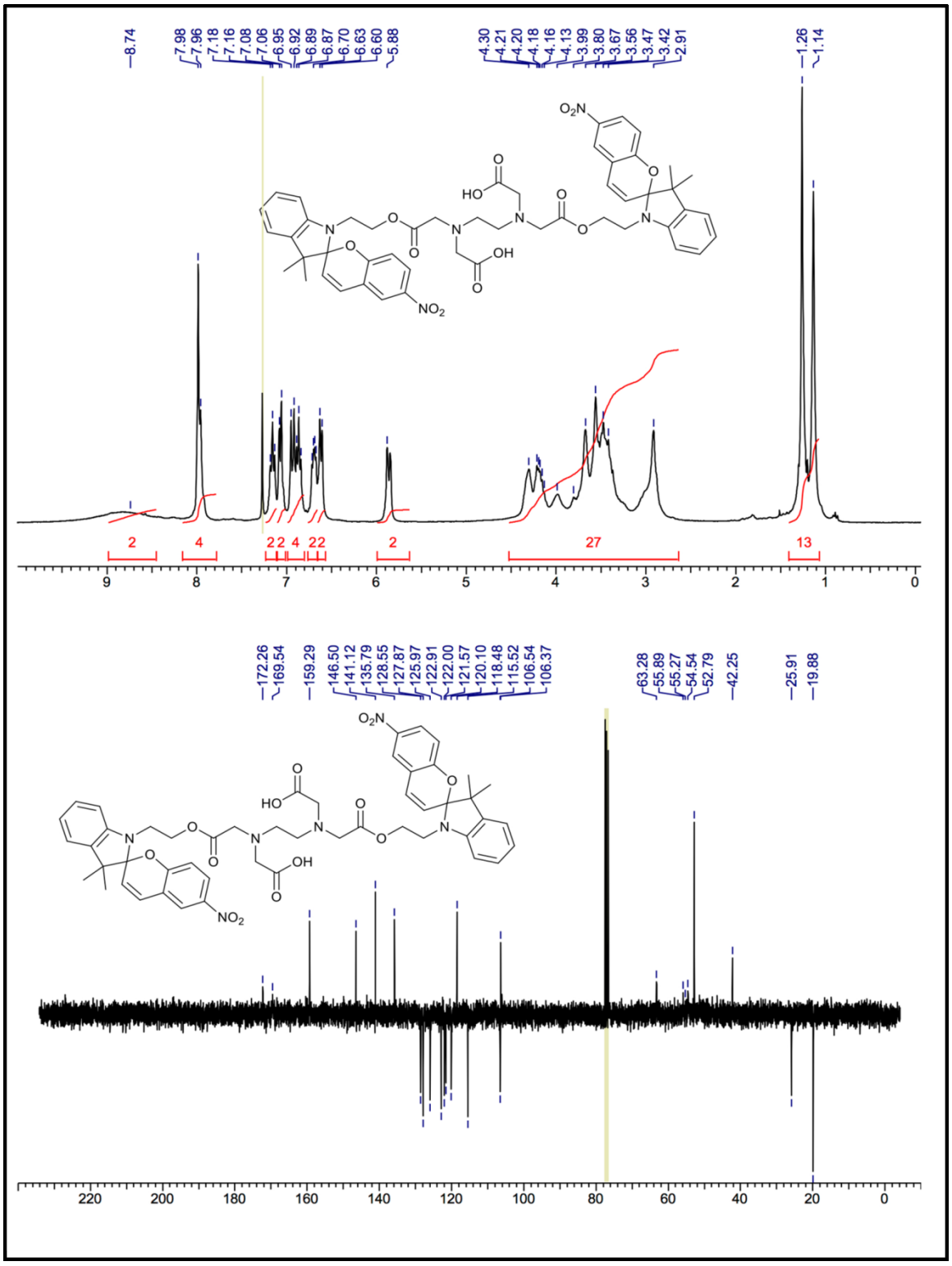

Figure 3.2. ^{1}H NMR (top) and ^{13}C NMR (bottom) of bis-spiropyran.

3.3. Results and Discussion

The oleate-capped $LiYF_4:Tm^{3+}$, Yb^{3+} UCNPs prepared via the thermal decomposition method show a diamond-like morphology (Figure 3.3) and are approximately 89 nm along the long axis with a narrow particle size distribution (Figure 3.4). XRPD analysis showed the highly crystalline nature of the material and confirmed the tetragonal structure of the $LiYF_4:Tm^{3+}$, Yb^{3+} UCNPs (Figure 3.5). Moreover, the upconversion luminescence spectrum upon irradiation with 980 nm light showed that the UCNPs emit strong UV light centered at 353 nm and 368 nm, which corresponds to the $^3P_0$ - $^3F_4$ and $^1D_2$ - $^3H_6$ transitions from the Tm^{3+} ions, respectively (in Figure 3.6).

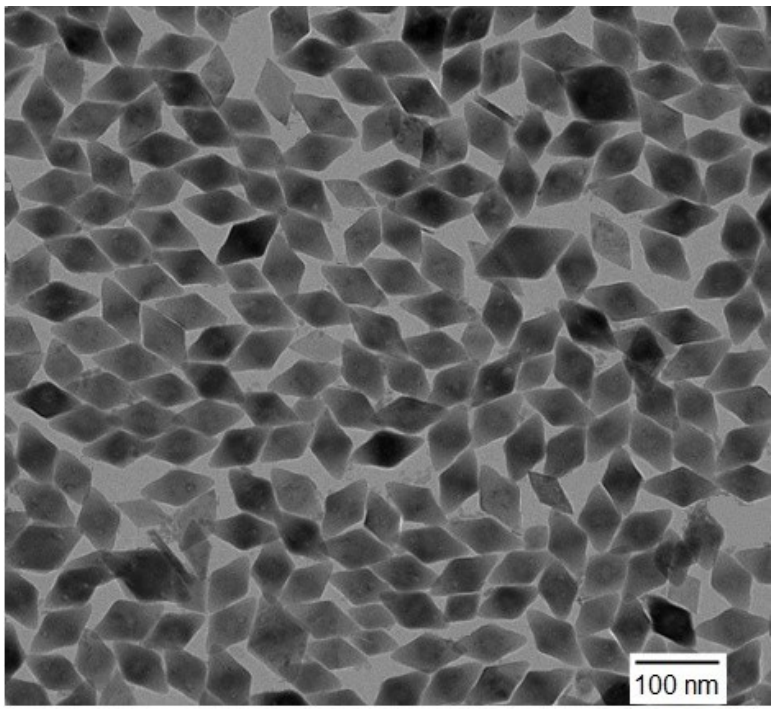

Figure 3.3. Transmission electron microscopy image of oleate-capped $LiYF_4$: Tm^{3+} 0.5 mol%, Yb^{3+} 25 mol% (1 wt% in toluene).

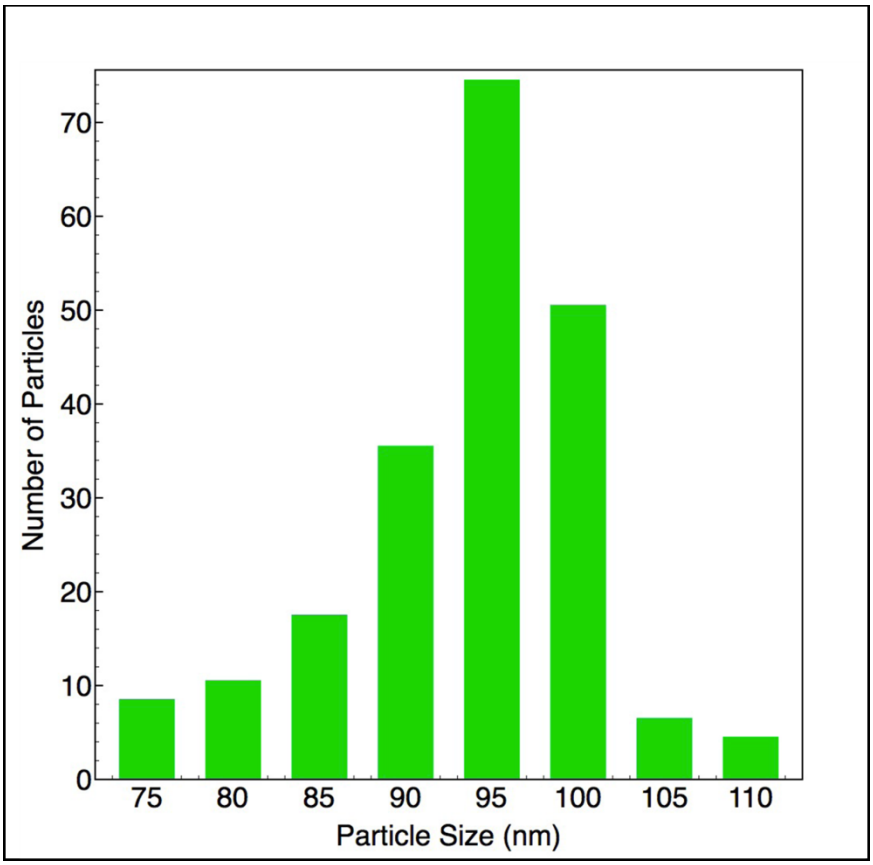

Figure 3.4. Particle size distribution of the oleate-capped $LiYF_4$: Tm^{3+} 0.5 mol%, Yb^{3+} 25 mol% obtained from the long axis. Average particle size was determined to be 89 nm.

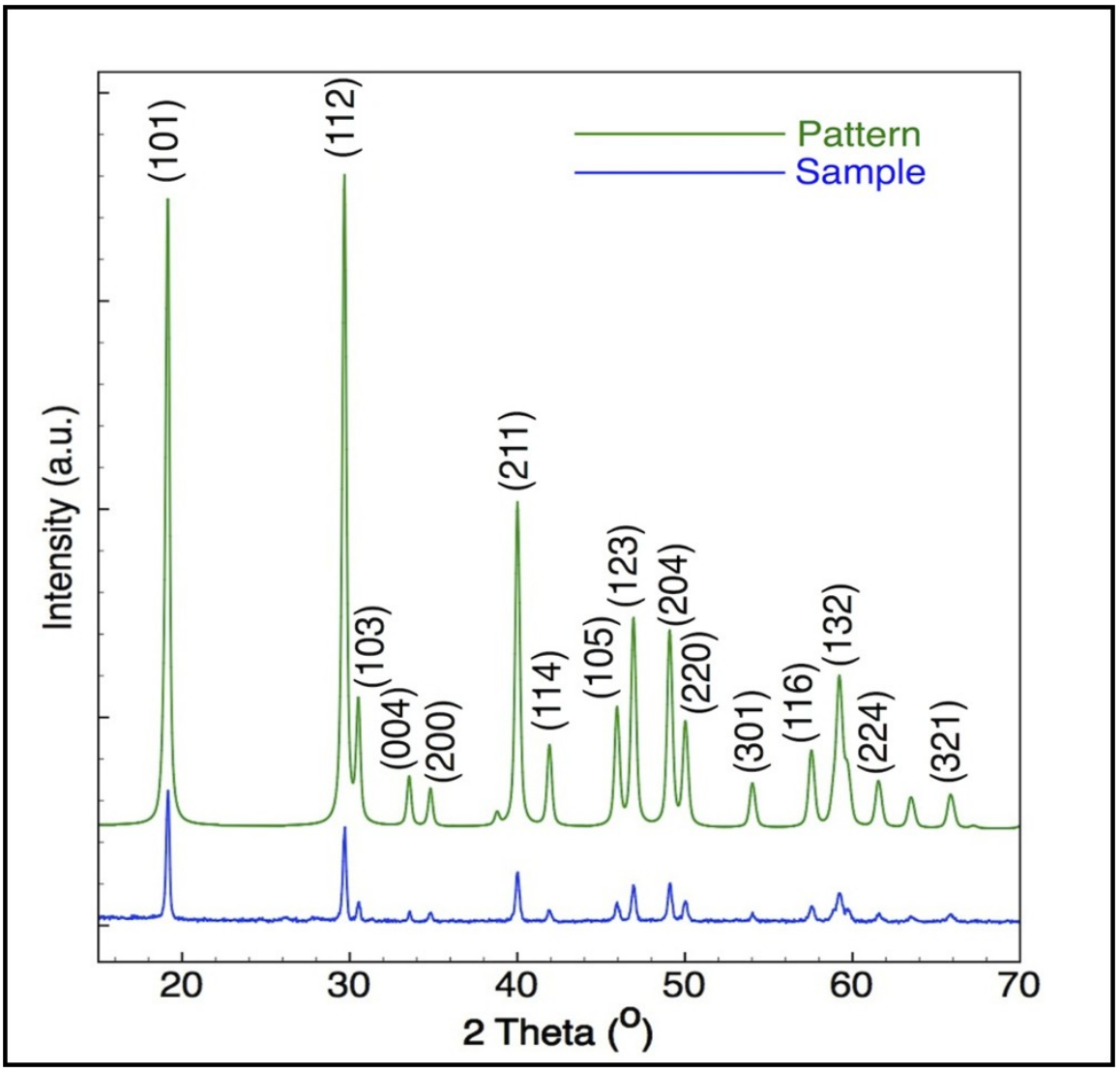

Figure 3.5. Experimental (blue line) and standard (green line) X-ray diffraction patterns for the oleate-capped $LiYF_4$: Tm^{3+} 0.5 mol%, Yb^{3+} 25 mol%.

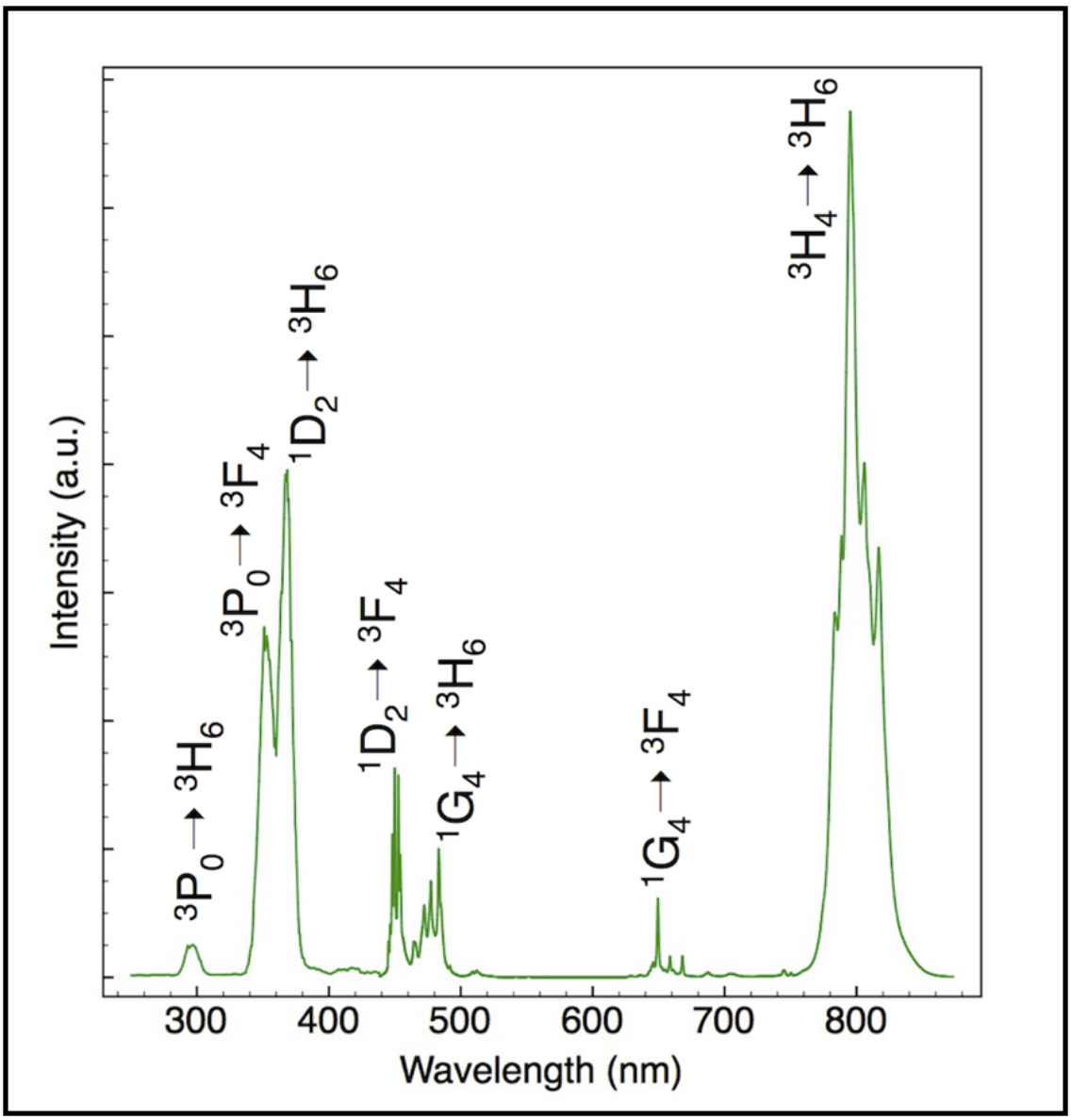

Figure 3.6. Upconversion luminescence spectrum of of oleate-capped $LiYF_4$: Tm^{3+} 0.5 mol%, Yb^{3+} 25 mol% in toluene excited at 980 nm.

In order to achieve the transformation from ring-closed bisspiropyran form to the ring-open merocyanine form *via* the upconverted UV emission of UCNPs, grafting the bis-spiropyran molecules onto the surface of the nanoparticles is imperative since it will enhance the energy transfer eficiency. The bis-spiropyran molecules will be sensitized *via* FRET, which is distance dependent. Thus, the spatial separation between donor (UCNPs)

and acceptor molecules (bis-spiropyran) should be small enough to favor efficient non-radiative transfer. In addition, the absorption peak of the ring-closed bis-spiropyran overlaps with the UV emission of the $LiYF_4:Tm^{3+}$, Yb^{3+} UCNPs centered at 353 nm and 368 nm from the $^3P_0$ - $^3F_4$ and $^1D_2$ - $^3H_6$ transitions of the Tm^{3+} ions, respectively (Figure 3.7). This yields the possibility of using the UCNPs as a UV source to trigger the bis-spiropyran → bis-merocyanine transformation. Thus, bygrafting these photochromic compounds onto the surface of the UCNPs via a ligand exchange process, we were able to generate the BSP-UCNP conjugate system (Figure 3.8).

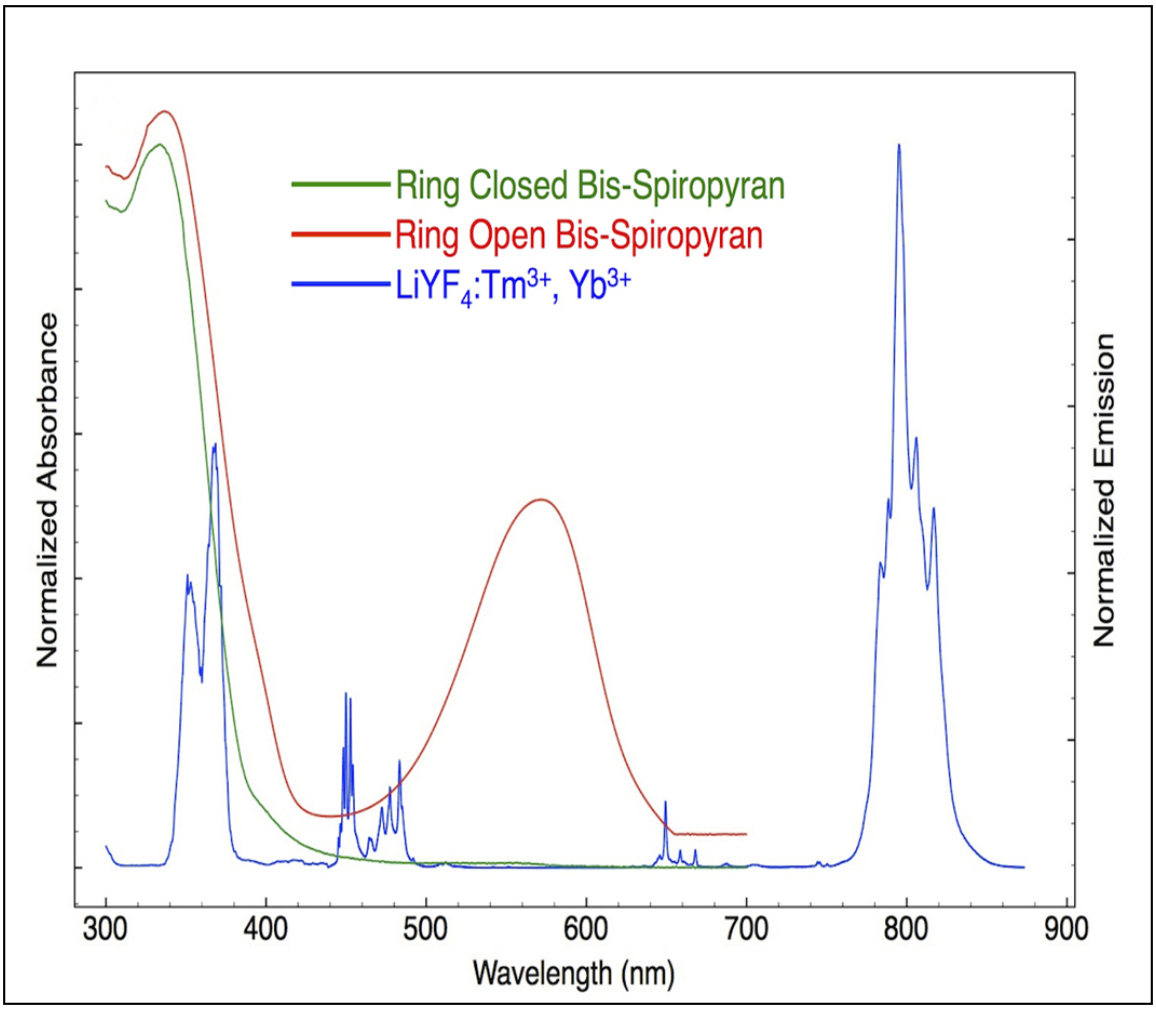

Figure 3.7. Absorption spectra of ring-closed spiropyran (green line) and ring-open merocyanine (red line) in THF solvent. The bis-spiropyran to bis-merocyanine transformation was achieved by irradiation at 365 nm. The blue curve represents the upconverting emission spectrum of $LiYF_4:Tm^{3+}$, Yb^{3+} UCNPs (excited at 980 nm) demonstrating the overlap of absorption and emission spectra.

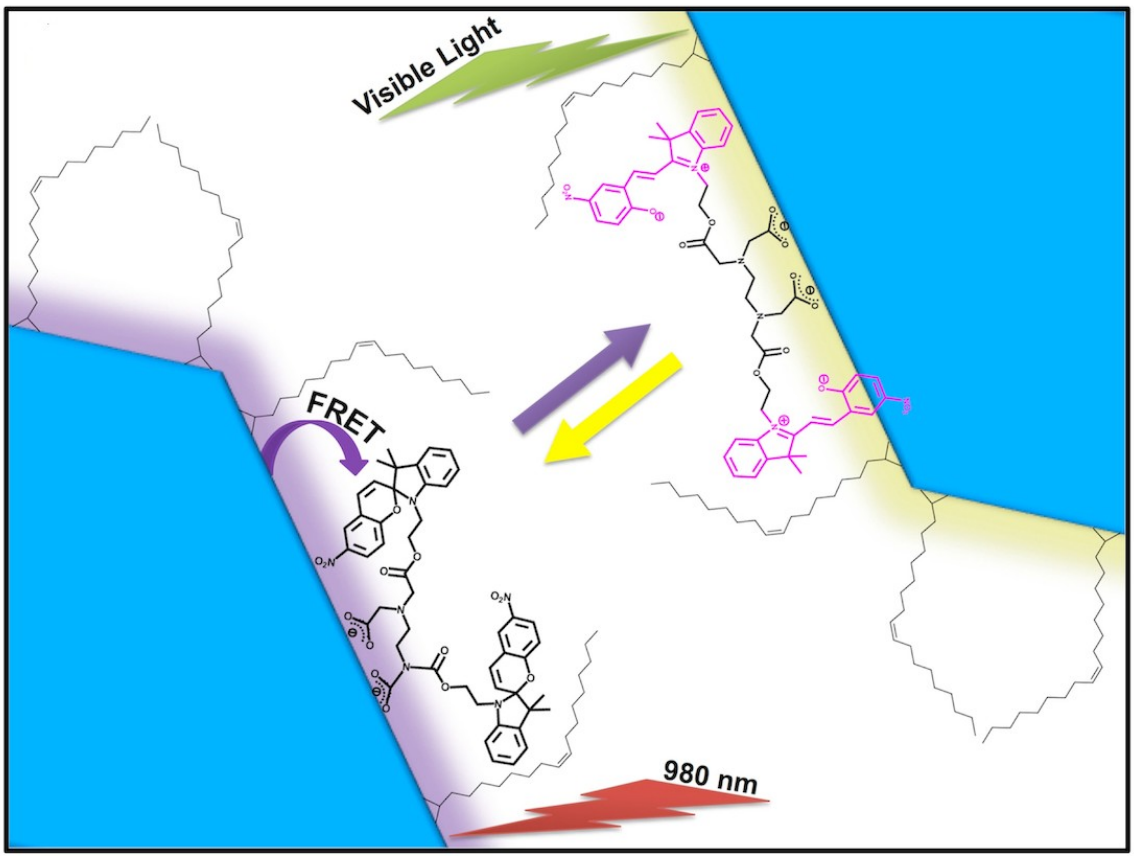

Figure 3.8. Molecular structures of the ringclosed and ring-open isomers of the bis-spiropyran and the photoinduced isomerization. The ring-closed colorless bis-spiropyran can be converted to ring-open colored bis-merocyanine under irradiation at 365 nm; the reverse photocyclization can be achieved by illumination of visible lightwith a wavelength > 500 nm. The schematic of photoswitching of bisspiropyran in the BSP-UCNPs system is presented.

To confirm the success of the ligand exchange process between the oleate capping ligand and the bis-spiropyran, we used FTIR spectroscopy to identify the functional groups before and after ligand exchange. By comparing the fingerprint region of the FTIR spectra between BSP-UCNPs (blue line) and bisspiropyran (green line), it clearly shows that bis-spiropyran was successfully grafted on the surface of the UCNPs (Figure 3.9). However, comparison of the spectra of oleate-capped UCNPs (red line) and BSP-UCNPs (blue line), make it difficult to conclude that the oleate is completely removed as some of the characteristic peaks attributed to the oleate such as carboxylate symmetric

stretching (at 1568 cm^{-1}) and asymmetric stretching (at 1468 cm^{-1}) are still present in the BSP-UCNPs spectrum. Thus, we concluded that the oleate capping ligands on the surface of the UCNPs were not completely exchanged by bis-spiropyran. It should also be noted that the ratio between the peaks at 1744 cm^{-1} (corresponding to –COOH) and 1690 cm^{-1} (corresponding to COO^-) in the spectrum of BSP-UCNPs decreased dramatically, compared to the spectrum of bis-spiropyran. This is indicative that some carboxylic groups were converted into carboxylate groups after ligand exchange demonstrating that the bis-spiropyran molecule was in fact grafted on to the surface of the UCNPs through carboxylate groups [67, 68].

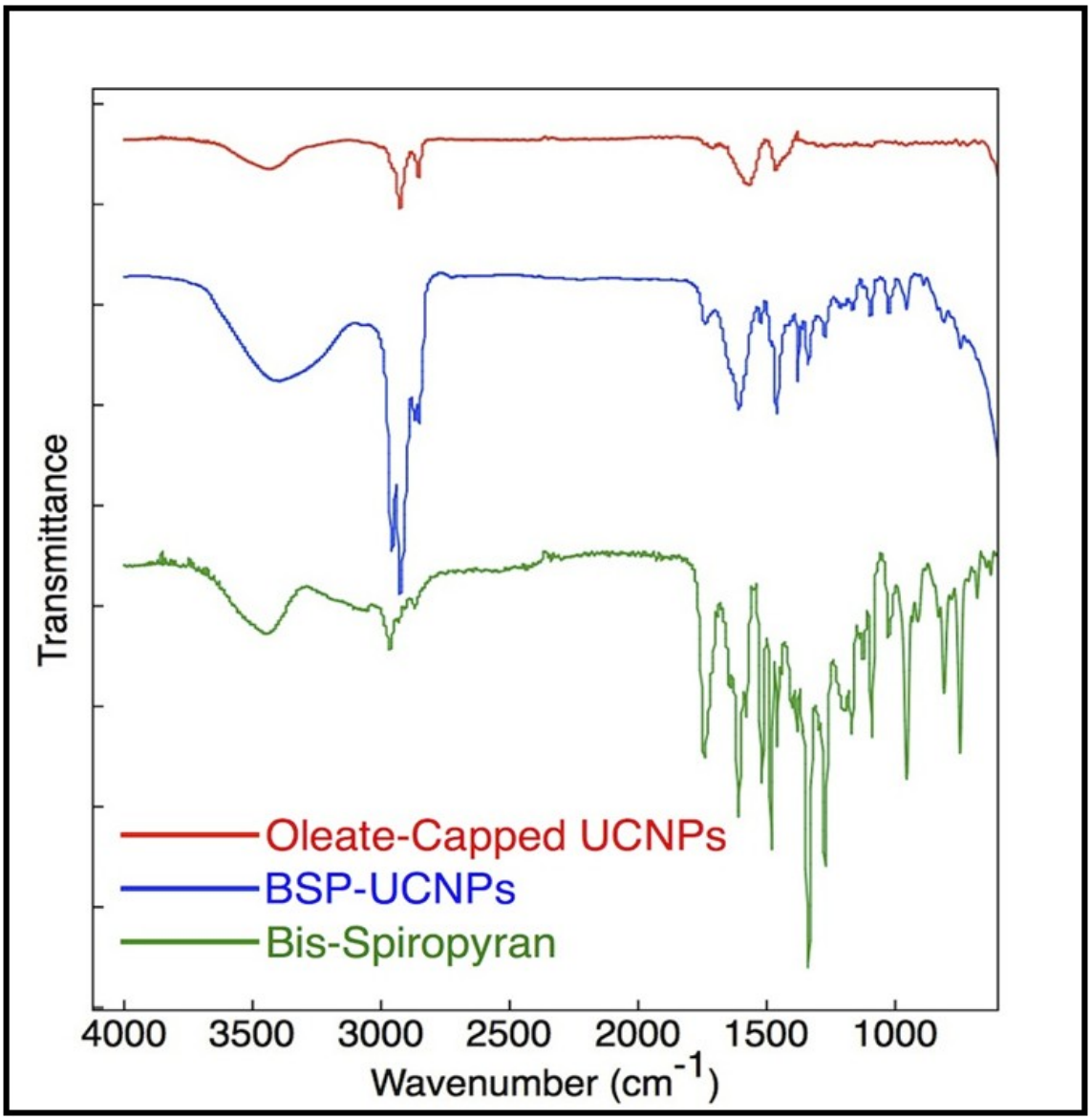

Figure 3.9. Fourier transform infrared spectra of oleate-capped UCNPs (red line); BSP-UCNPs (blue line); and bis-spiropyran (green line).

To determine the concentration of bis-spiropyran on the surface of the UCNPs, we measured its absorbance in THF at 333 nm and established a calibration curve. Using this curve and the absorbance value obtained for a sample of 0.2 wt% BSP-UCNPs, we found the concentration of bis-spiropyran on the nanoparticles to be 6.8×10^{-5} M (see Figure 3.10), which represents approximately 220 molecules of bis-spiropyran on the surface of the UCNPs.

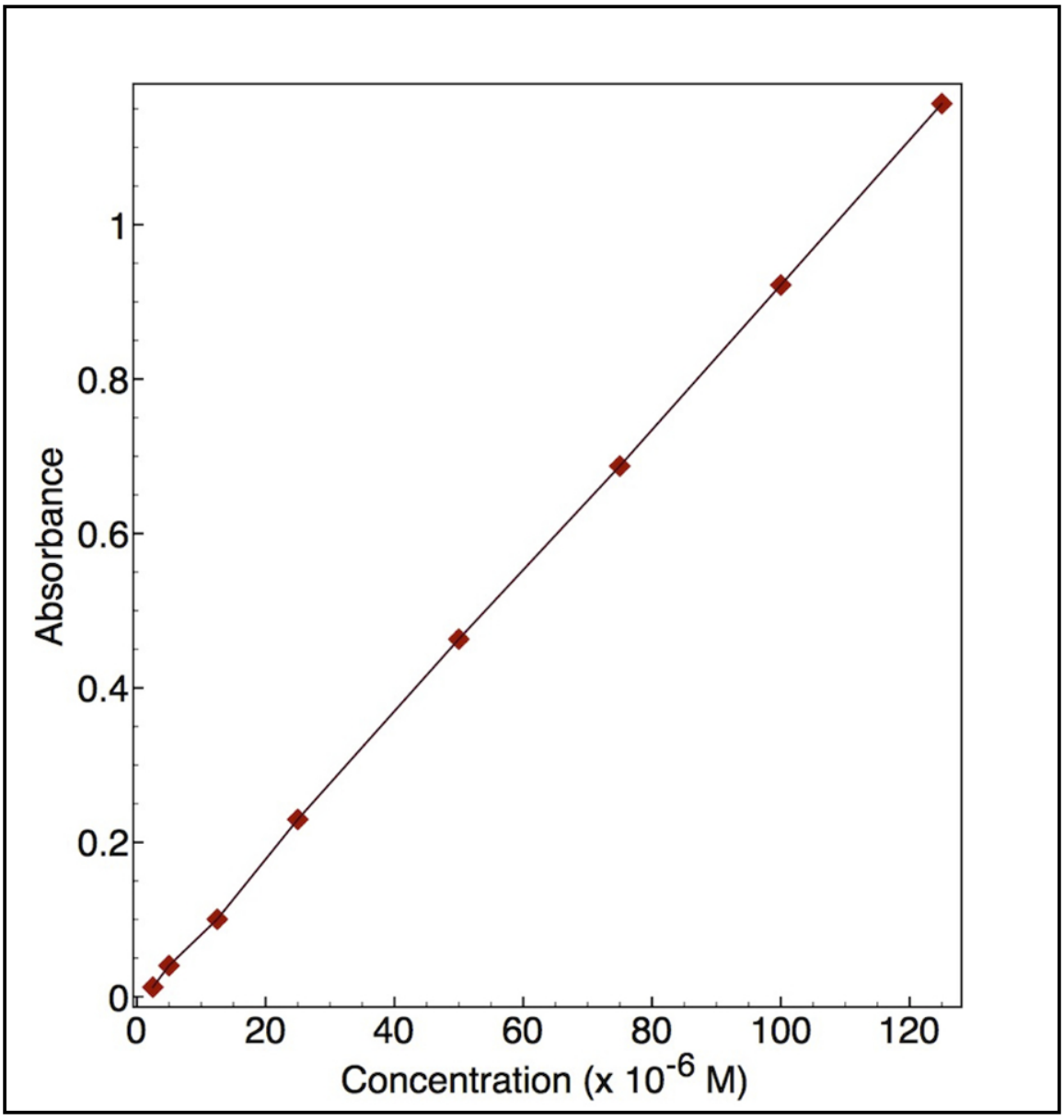

Figure 3.10. Calibration curve of bis-spiropyran in THF (absorbance at 333 nm). The concentration of bisspiropyranwas determined to be 6.8 x 10^{-5} M in a solution of 0.2 wt% BSP-UCNPs in THF.

Figure 3.11 shows the upconversion spectra of oleate-capped UCNPs (0.2 wt% in THF), BSP-UCNPs (0.2 wt% in THF) and a solution of 0.2 wt% oleate-capped UCNPs plus 6.8 x 10^{-5} M of bisspiropyran in THF. We observe a significant difference in the intensity of the UV peaks centered at 353 and 368 nm of the BSP-UCNPs (bis-spiropyran

functionalized on the UCNPs) in comparison to the respective peaks for the oleate-capped UCNPs and the solution of oleate-capped UCNPs and bis-spiropyran.

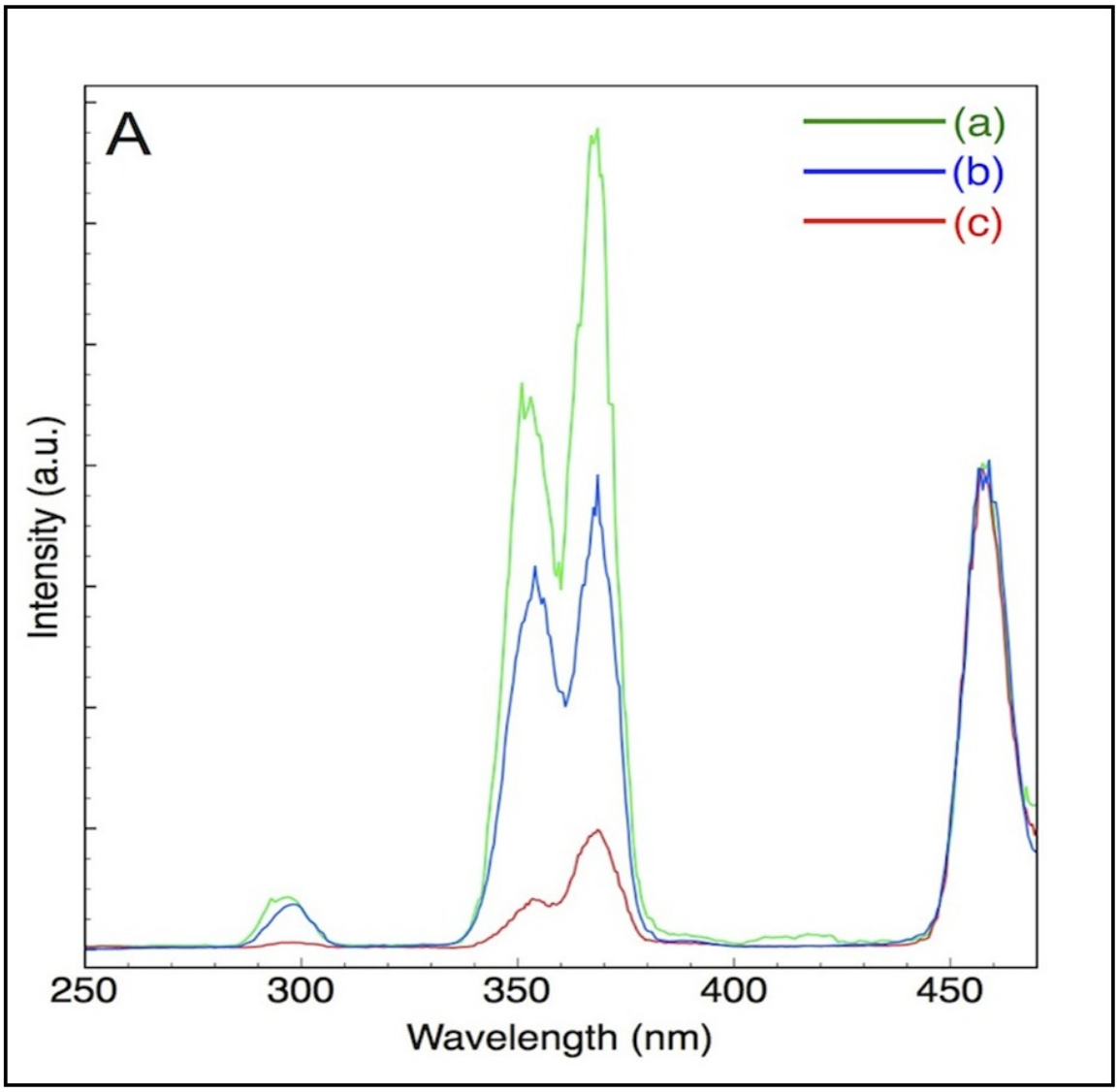

Figure 3.11. Upconverting emission spectra following excitation at 980 nm demonstrating the quenching of the UV emission through a FRET process to bis-spiropyran; (a) Oleate-capped UCNPs (0.2 wt% in THF); (b) Simple mixture consisting of 0.2 wt% oleate-capped UCNPs and 6.8 x 10^{-5} M of bis-spiropyran in THF; (c) BSP-UCNPs (0.2 wt % in THF).

This provides evidence of a possible non-radiative energy transfer from the UCNPs to the bis-spiropyran. Subsequently, the energy transfer efficiency was calculated using the following equation [69],

$$E = 1 - \frac{I_1}{I_2} \qquad (3.1)$$

Where E is the energy transfer efficiency, I_1 is the intensity of BSP-UCNPs or the mixture of oleate capped UCNPs plus BSP sample at 368 nm, and I_2 is the intensity of oleate-capped UCNPs at 368 nm. The calculated energy transfer efficiency for the BSP-UCNPs was determined to be 81% whereas for the solution (oleate-capped UCNPs plus bis-spiropyran), the energy transfer efficiency was calculated to be 42%. These results confirm that the distance separating the bis-spiropyran molecules on the UCNPs in the bis-spiropyran functionalized UCNPs system is far smaller than that of the solution of the oleate-capped UCNPs and bis-spiropyran, in which the bis-spiropyran molecules are moving randomly in the solution. This suggests that the bis-spiropyan molecules in BSP-UCNP system are indeed capping the surface of the UCNPs and readily undergo an efficient FRET process.

Kinetic studies were performed in order to evaluate the effect that the functionalization of bis-spiropyran on the UCNPs has on the ring opening kinetics of the bis-spiropyran, which is known to be first order [70]. This involved irradiation of a 50 μL solution of 1 wt% BSP-UCNPs in THF under NIR excitation (980 nm) and recording the absorbance value of the bis-merocyanine at λmax =570 nm at intervals of 30 s (in the range of 0-240 s) (Figure 3.12).

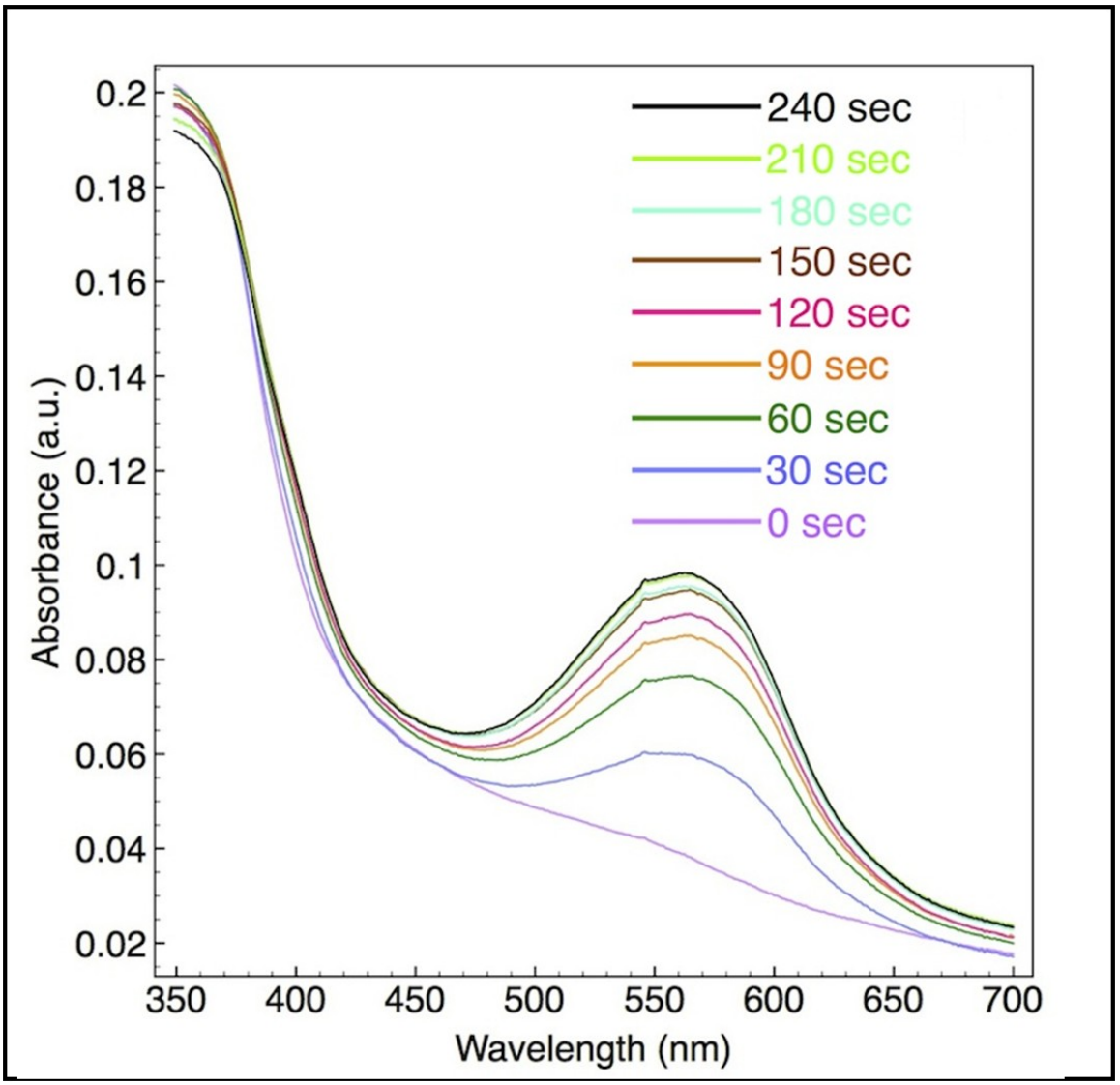

Figure 3.12. UV-Vis absorption spectra of BSP-UCNPs (1 wt% in THF, 50 µL) after irradiation with 980 nm laser light at 30 second intervals.

This allowed us to calculate the rate constant of the bisspiropyran to bis-merocyanine transformation (see Figure 3.13 and Figure 3.14) using the following equation [71]:

$$\ln\left(\frac{A_f - A_o}{A_f - A_t}\right) = kt \qquad (3.2)$$

Where A_f is the absorbance at infinite time, A_0 is the absorbance 25 at $t = 0$, and A_t is the absorbance following 980 nm irradiation at every interval; k is the rate constant,

and *t* is the irradiation time. Our results show that ring-closed to ring-open isomerisation reaction follows first order kinetics with a rate constant $k = 1.9 \times 10^{-2}\ s^{-1}$ which is in good agreement with the values reported for the conversion of spiropyran to merocyanine in non-polar solvents [13] (Figure 3.14). The results show that the ring opening is fast and with a $t_{1/2} = 53s$ for the conversion of bis-spiropyran to bismerocyanine on the UCNPs using NIR light irradiation.

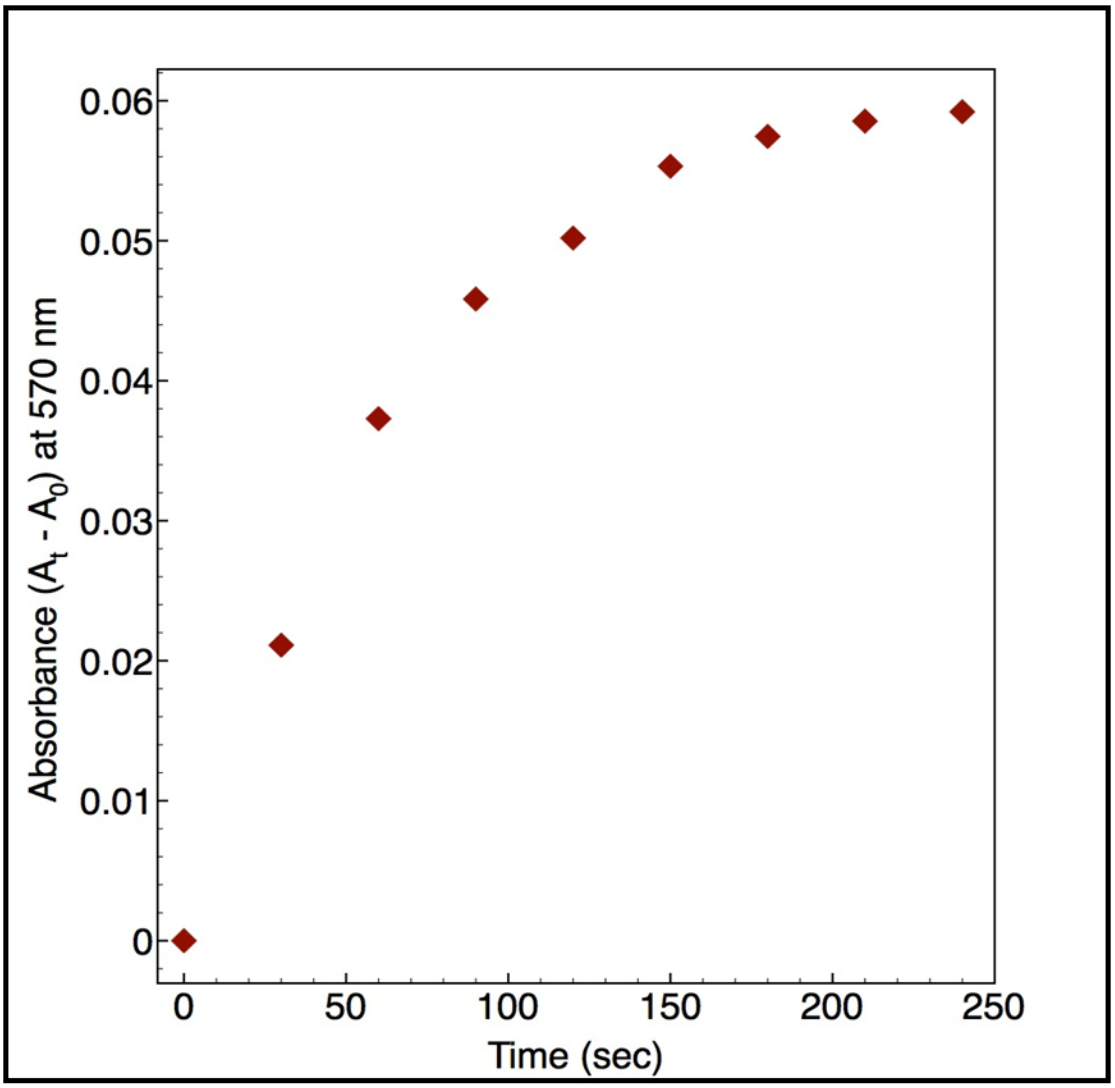

Figure 3.13. Kinetic curve of BSP-UCNPs following 980 nm laser irradiation (at 570 nm).

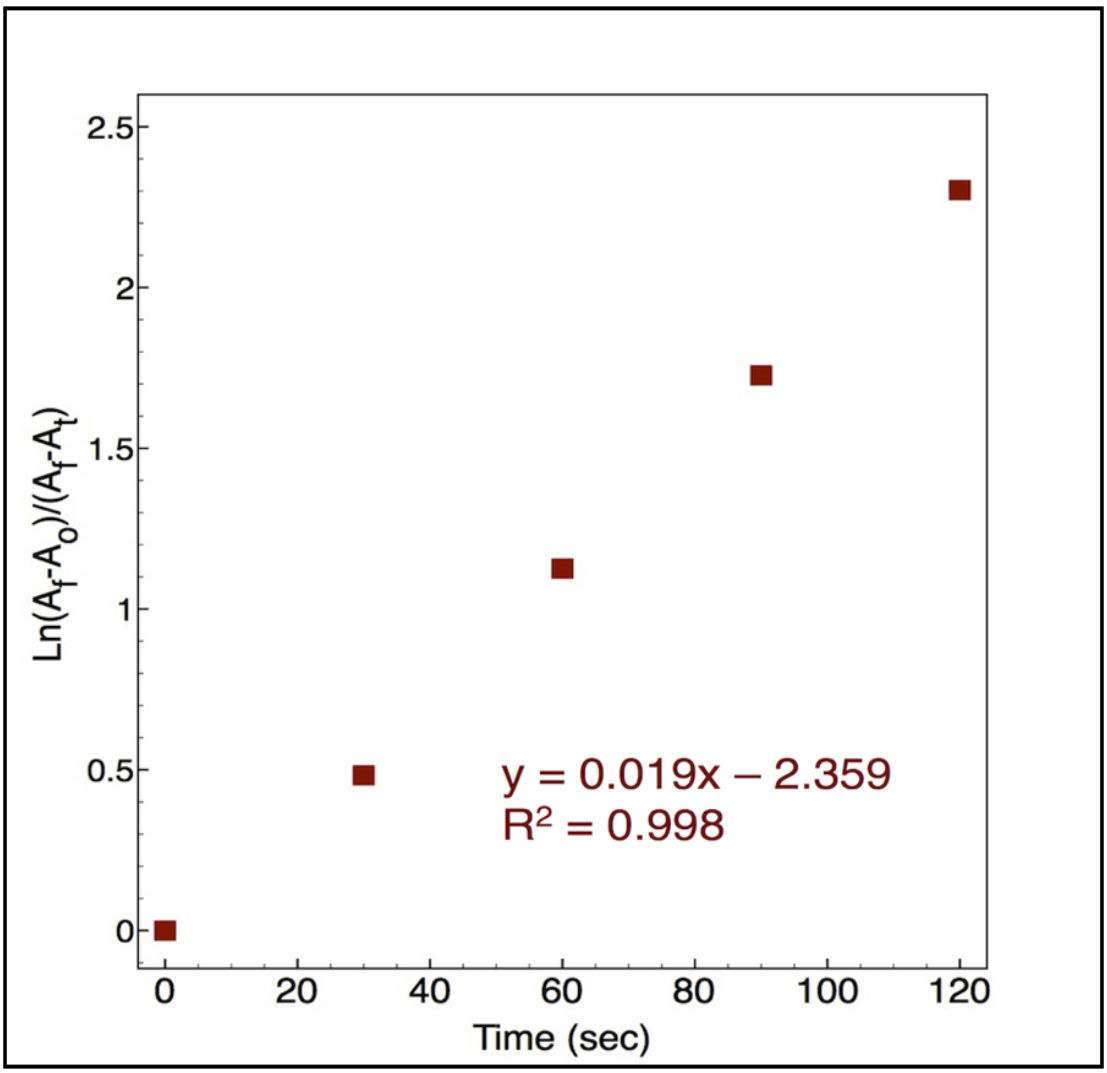

Figure 3.14. Reaction order determination A_0, A_t and A_f: absorbance at t = 0, t, infinite time, respectively.

Photodegradation of many organic photochromic molecules is a well known phenomenon which occurs when these molecules are repeatedly switched between two forms, using UV radiation, over a certain number of times (cycles). To investigate the photostability we monitored the absorbance of the peak at 580 nm while continuously switching between the BSP-UCNPs and bis-merocyanine-UCNPs (BMC-UCNPs). Figure 3.15A shows the absorbance measured at 570 nm for the cyclical switching between BSP-UCNPs and BMC-UCNPs when exposed to 365 nm light for 30 seconds followed

by irradiation with visible light for 30 seconds. Figure 3.15B shows the results obtained when using 980 nm excitation followed by visible irradiation. As shown in Fig. 3.15A, B switching with UV and visible light is reversible and does not adversely affect the efficiency of the switching.

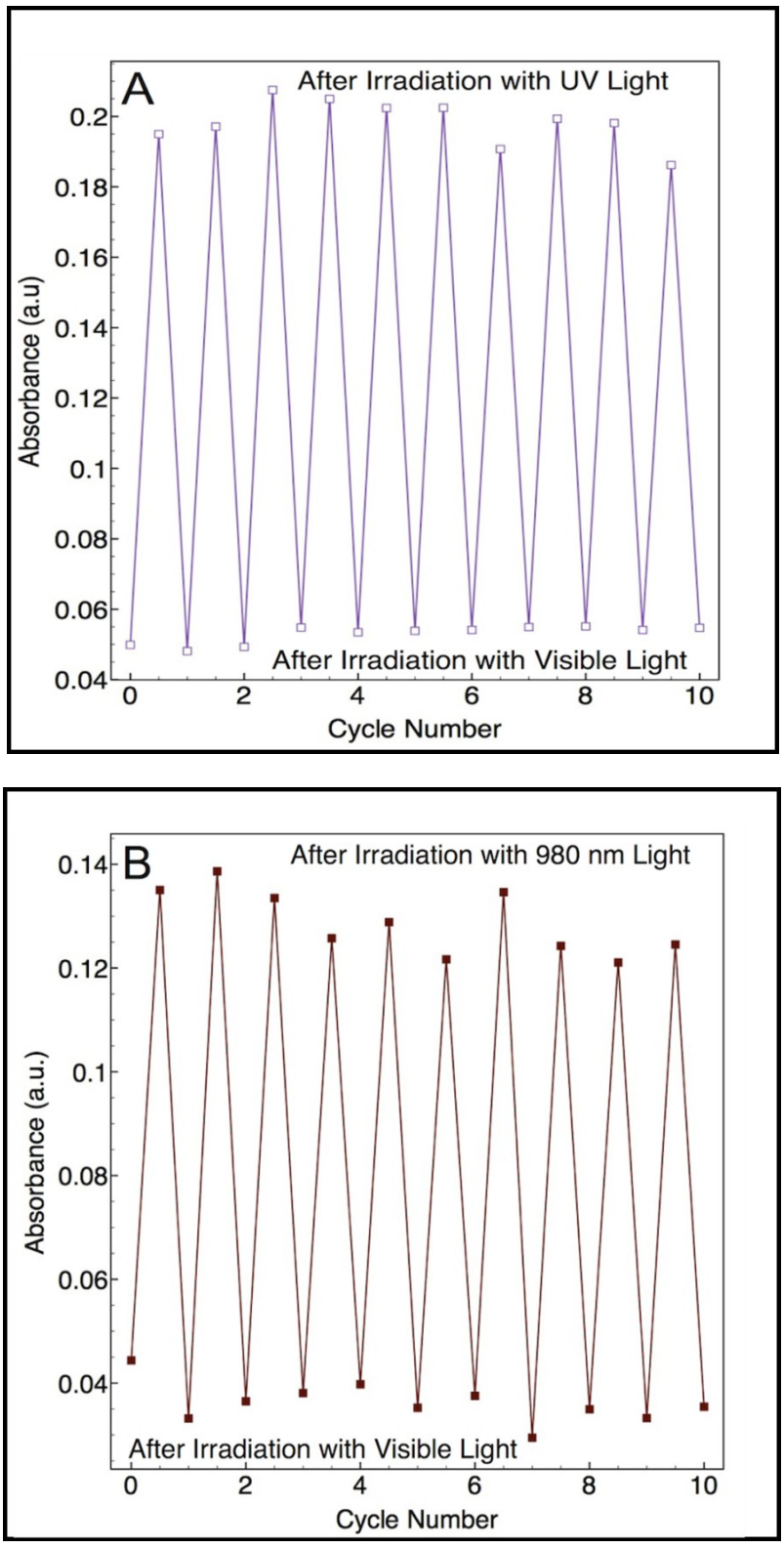

Figure 3.15. (A) Irradiation cycles of BSP-UCNPs (1 wt% in THF) under alternate UV (365 nm; 30 s) and visible (30 s) light irradiation; (B) Irradiation cycles of BSP-UCNPs (1 wt% in THF) under alternate 980 nm (3 min.) and visible (30 s) light irradiation.

3.4. Experimental

3.4.1. Synthesis of $LiYF_4:Tm^{3+}$, Yb^{3+} (UCNPs)

Thulium oxide (Tm_2O_3, 99.99+ %), ytterbium oxide (Yb_2O_3, 99.99%), yttrium oxide (Y_2O_3, 99.99+ %), trifluoroacetic acid (CF3COOH, 99%), lithium trifluoroacetate (CF_3COOLi, 98%), oleic acid (technical grade, 90%), and 1-octadecene (technical grade, 90%) were all purchased from Sigma-Aldrich and were used without further purification. $LiYF_4:Tm^{3+}$, Yb^{3+} UCNPs were synthesized via thethermal decomposition method previously demonstrated by our group [30, 72-73], which was comprised of a two-step process. In the first step, a 10 mL mixture of water/trifluoroacetic acid (1:1) was added to around-bottom flask containing 6.25×10^{-6} mol of Tm_2O_3 (0.0024 g, 0.5 mol % Tm^{3+}), 3.13×10^{-4} mol of Yb_2O_3 (0.1232 g, 25 mol % Yb^{3+}), and 9.31×10^{-4} mol of Y_2O_3 (0.2103 g), and the cloudy solution was heated to reflux at 80 °C until it was clear. The resulting solution was then dried at 60 °C to form the trifluoroacetate lanthanide precursors. In the second step, 12.5 mL of oleic acid and 12.5 mL of 1-octadecene were added to a 3-neck round bottom flask (solution A) and degassed at 150 °C for 30 min, and then maintained at the same temperature under argon atmosphere. Approximately 2.50×10^{-3} mol (0.2999 g) of CF_3COOLi was added to the dried precursor solids along with 7.5 mL of oleic acid and 7.5 mL of 1-octadecene (solution B), the resulting solution was degassed at 45 °C, 75 °C, and 125 °C for 5 min, respectively. Meanwhile, solution A was heated to 315 °C. At this moment, solution B was injected into solution using a syringe and pump system at a rate of 1.5 mL/min (Harvard Apparatus Econoflow). The reaction mixture was left to stir vigorously for 90 min under argon gas. After cooling down to room temperature, absolute ethanol was added to the reaction solution to

precipitate UCNPs, which were subsequently isolated *via* centrifugation (3000 rpm, 15 min). The pellets were washed with a 1:3 hexane/ethanol mixture twice to remove any impurities.

3.4.2. Synthesis of Bis-Spiropyran

1-(2-Hydroxyethyl)-3,3-dimethylindolino-6'-nitrobenzopyrylospiran (200 mg, 0.57 mmol) and Ethylenediaminetetraacetic dianhydride (73 mg, 0.285 mmol) were dissolved in 5 mL of anhydrous DMF in an inert atmosphere. The solution mixture was heated to 80 °C for 24 h. Subsequently, the solution was allowed to cool to room temperature and water was added to precipitate the compound, which was subsequently isolated by filtration and dried under vacuum. The target molecule was obtained as a pinkish solid in an 80 % yield.

3.4.3. Ligand Exchange Reaction with Bis-Spiropyran

UCNPs conjugated with bis-spiropyran (BSP-UCNPs) were synthesized by a ligand exchange reaction between oleate-capped UCNPs ($LiYF_4$:Tm^{3+}, Yb^{3+}) and bis-spiropyran. Typically, 100 mg of UCNPs were dispersed in 5 mL tetrahydrofuran (THF) followed by the addition of 10 mg of bis-spiropyran in 1 mL of THF. The mixture was stirred at room temperature for 48 h and the resulting solution was subsequently centrifuged at 3000 rpm for 15 min. After centrifugation the clear supernatant was eliminated and the pellet was re-dispersed with THF and washed twice. Free unbound bis-spiropyran molecules were removed by further centrifugations and the resulting pink deposit was subsequently dispersed in THF for use.

3.4.4. Characterization

3.4.4.1. Fourier Transform Infrared (FTIR) Spectroscopy

FTIR spectra of the as-synthesized bis-spiropyran molecules, oleate-capped UCNPs, and the BSP-UCNPs conjugate were measured on a Nicolet 6700 FTIR spectrometer in KBr pellets.

3.4.4.2. Transmission Electron Microscopy (TEM)

TEM analysis of the colloidal dispersion of UCNPs were performed using a Philips CM200 microscope operating at 200 kV equipped with a charge-coupled device (CCD) camera (Gatan). Prior to analysis, a 20 mg sample was dispersed in 2 g of toluene to yield an approximate 1 wt% solution. A few drops of the resulting solution were evaporated on a formvar/carbon film supported on a 300 mesh copper grid (3 mm in diameter).

3.4.4.3. X-Ray Powder Diffraction (XRPD)

XRPD patterns were measured using a Scintag XDS-2000 Diffractometer equipped with a Si(Li) Peltier-cooled solid state detector, Cu Kα source at a generator power of 45 kV and 40 mA, divergent beam (2 mm and 4 mm), and receiving beam slits (0.5 mm and 0.2 mm). The scan range was set from 20-80° 2θ with a step size of 0.02° and a count time of 2 s. The sample was measured using a quartz “zero background” disk.

3.4.4.4. Upconversion Luminescence Spectroscopy

The upconversion visible emission spectra of the oleate-capped UCNPs and the BSP-UCNPs were obtained upon 980 nm excitation, using a Coherent 6-pin fiber-coupled F6 series 980 nm laser diode (power of 615 mW), coupled to a 100 μm (core) fiber. For the upconversion studies, the samples (1 wt% in THF) were placed in 1 cm

path-length quartz cuvettes (Hellma, QS). The upconverted visibleemissions were collected at right angles with respect to the incident beam and subsequently dispersed by a 1m Jarrell-Ash Czerny-Turner double monochromator with an optical resolution of ~0.15 nm. The visible emissions were detected by a thermoelectrically cooled Hamamatsu R943-02 photomultiplier tube. A preamplifier, model SR440 Standard Research Systems, processed the photomultiplier signals and a gated photon counter model SR400 Standard Research Systems data acquisition system was used as an interface between the computer and the spectroscopic hardware. The signal was recorded under computer control using the Standard Research Systems SR465 software data acquisition/analyzer system.

The UV emissions were collected using a Spex Minimate 1/4 m monochromator and detected with an Oriel 70680 photomultiplier tube. It should be noted that while the UV and visible emissions are measured with different detectors, they do in fact have overlapping wavelengths in the blue region. Thus, by measuring the overlapping regions with both monochromators, under identical conditions, the intensity of the UV emissions could be compared to the visible ones.

3.4.4.5. UV-visible absorption measurement

UV-visible absorption spectra of bis-spiropyran and BSP-UCNPs in THF solvent were recorded using Varian (Mulgrave, Victoria, Australia) Cary 5 and 5000 spectrophotometers.

3.5. Conclusion

In conclusion, by grafting bis-spiropyran molecules onto the surface of the oleate-capped UCNPs via ligand exchange, we demonstrated that fluorescence resonance energy

transfer from the upconverting UCNPs to the surface bis-spiropyran molecules can trigger the transformation of the ring-closed bis-spiropyran form to the ring-open bis-merocyanine form. Furthermore, the photochromic bis-spiropyran molecules in this system can be turned on and off using alternating NIR and visible light irradiation. Since the transformation in this model system was achieved by using NIR/visible excitation, along with the reasonable switching cycles, this new system would be veryuseful for biological applications related to photoswitching of photochromic compounds, which require UV irradiation to achieve the photochromic transformation.

Chapter Four - Conclusions and Future Work

4.1. Conclusions

Tm^{3+}/Yb^{3+} co-doped $LiYF_4$: (Tm^{3+} 0.5%, Yb^{3+} 25%) nanoparticles were successfully prepared via thermal decomposition method using the following optimized conditions: 1) reaction temperature 315 ºC; 2) reaction time of 90 minutes; and 3) precursor solution injection rate of 1.5 mL/min. Transmission electron microscopy (TEM) showed that the as-synthesized UCNPs were monodispersible in non-polar solvents, and had a diamond-like morphology and are approximately 89 nm, along the long axis with a narrow particle size distribution. These UCNPs also showed strong UV emission upon NIR (980 nm) excitation.

Via ligand exchange bis-spiropyran molecules were grafted onto the surface of the oleate-capped UCNPs. We demonstrated that bis-spiropyran molecules were successfully capped on the surface of the nanoparticles using Founier transform infrared spectroscopy (FTIR). The number of bis-spiropyran molecules on the surface of each nanoparticle was shown to be 220.

We also demonstrated that fluorescence resonance energy transfer from the upconverting UCNPs to the surface bis-spiropyran molecules can trigger the transformation of the ring-closed bis-spiropyran form to the ring-open bis-merocyanine form. Furthermore, the photochromic bis-spiropyran molecules in this system can be turned on and off using alternating NIR and visible light irradiation.

We also carried out a kinetic study of the ring opening photoswitching of BSP-UCNPs conjugate and showed that this process is a first order reaction under NIR excitation.

A fatigue test evidenced that the photodegradation of the bis-spiropyran functionalized UCNPs is negligible after ten cycles of switching on/off using NIR and visible light excitation.

Since the transformation in this model system was achieved by using NIR/visible excitation, along with the reasonable switching cycles, this new system would be very useful for biological applications related to photoswitching of photochromic compounds, which require UV irradiation to achieve the photochromic transformation.

4.2. Future Work

Although this model system suggests potential applications in biological system, the hydrophobic property of this hybrid prevents its direct application *in vivo*. Further modification to render this model system water dispersible should be carried out.

For this purpose, the BSP-UCNPs should be capped with an amphiphilic polymer molecule to form a shell on the surface. Figure 4.1 shows the structure of the amphiphilic polymer----poly(maleic anhydride alt-1-octadecene) (PMAO) [75, 76].

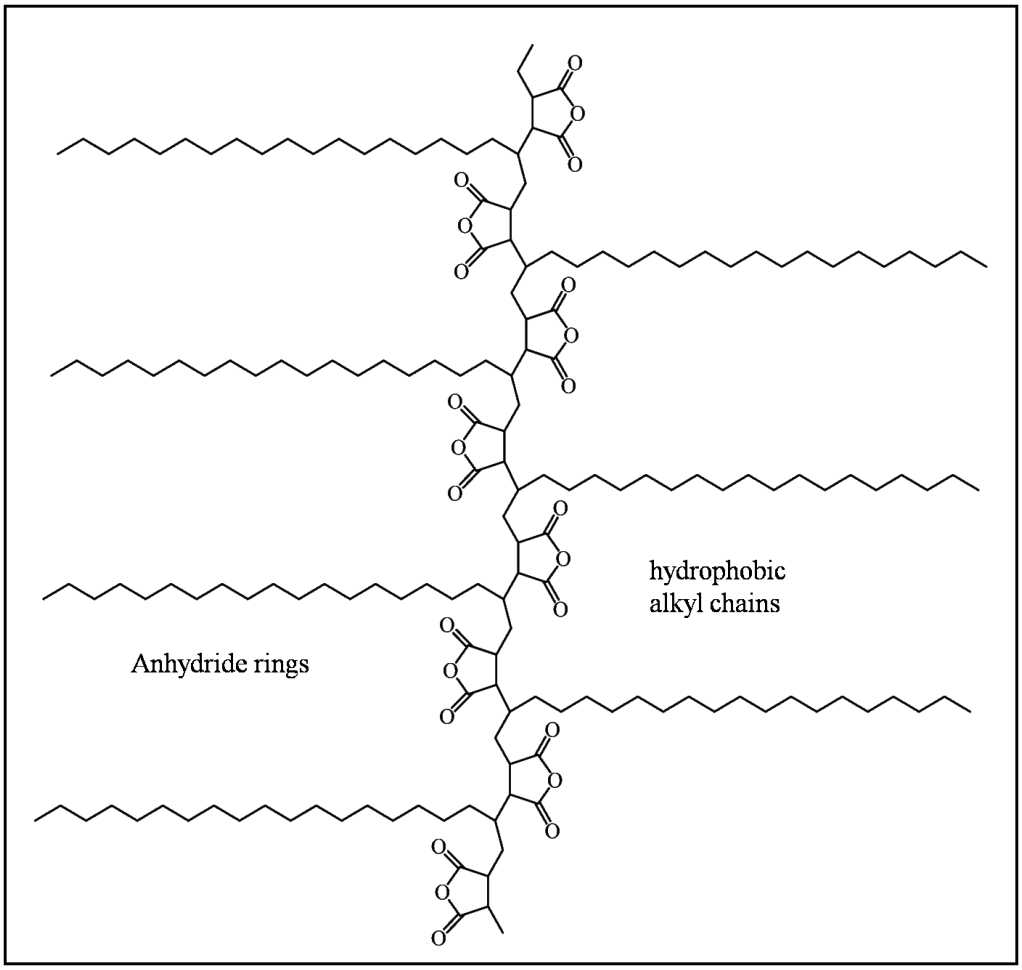

Figure 4.1. Structure of poly (maleic anhydride alt-1-octadecene) (PMAO).

The hydrophobic alkyl chains of the polymer are expected to interact with the hydrophobic bis-spiropyran molecule capping the UCNPs. After hydrolysis, the hyphophilic carboxylate groups of the polymer will form an outer shell, rendering this modified system water-dispersible [75-76]. The schematic representation of the polymer-coated BSP-UCNPs is illustrated in Figure 4.2.

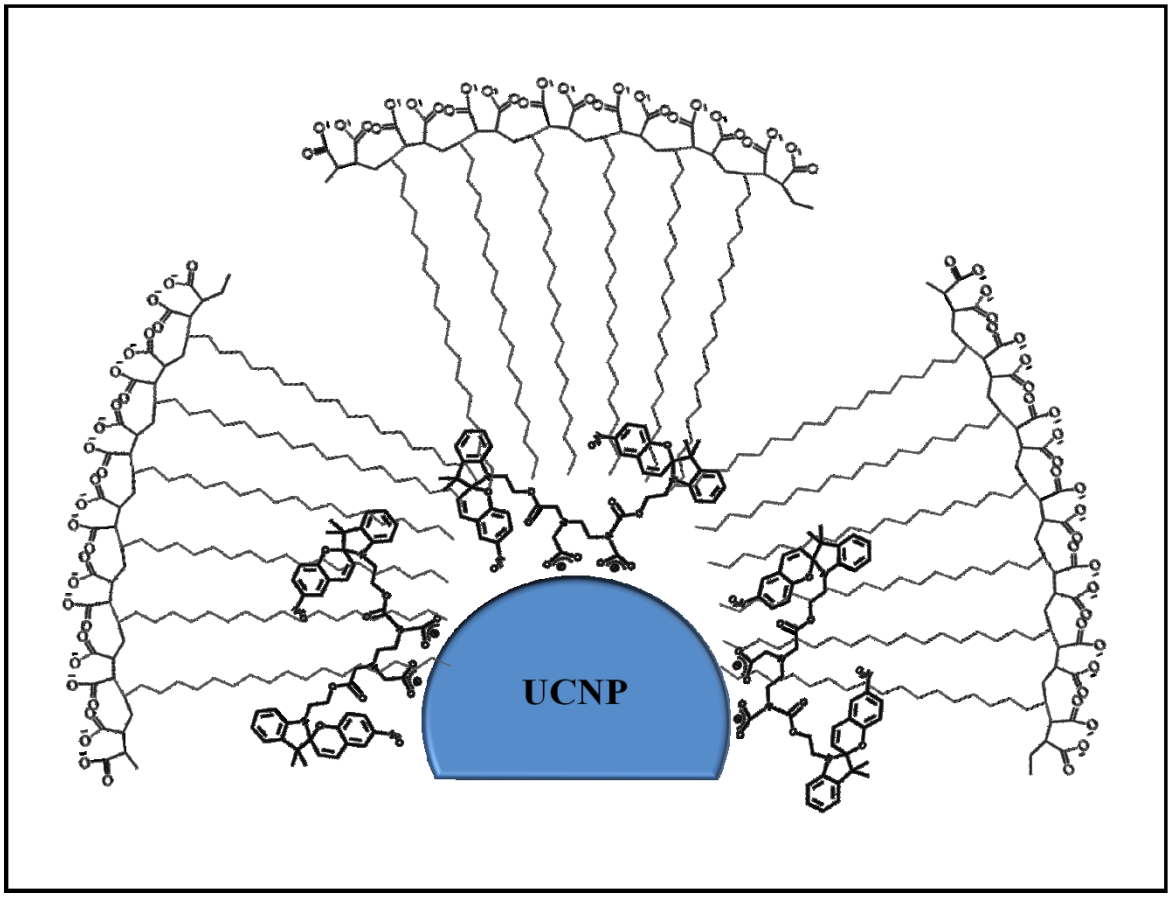

Figure 4.2. Schematic representation of polymer-coated BSP-UCNPs.

Further work should be carried out to investigate the photochromic efficiency of the water-dispersible conjugate.

References

1. G. H. Brown (Ed.), ***Photochromism*** (Wiley-Intersciences, New York, 1971).

2. J. C. Crano and R. J. Guglielmetti, ***Organic Photochromic and Thermochromic Compounds*** (Plenum Press, New York, 1999).

3. H. Dürr and H. Bouas-Laurent, ***Photochromism: Molecules and Systems*** (Elsevier, Amsterdam, 1990).

4. H. Bouas-Laurent and H. Dürr**,** ***Pure Appl. Chem.***, 2001, **4**, 639.

5. R. Pardo, M. Zayat and D. Levy, ***Chem. Soc. Rev.***, 2011, **40**, 672.

6. K. Kinashi, S. Nakamura, Y. Ono, K. Ishida and Y. Ueda, ***J. Photochem. Photobiol., A: Chemistry***, 2010, **213**, 136.

7. B. S. Lukyanov and M. B. Lukyanova, ***Chem. Heterocycl. Compd.,*** 2005, **3**, 281.

8. K. Goudjil, ***US Patent 5581090***, 1996.

9. S. Venkatramani and W. Kokonaski, ***US Patent 59141***, 1999.

10. Ryojiro and M. Takashi, ***US Patent 5644416***, 1997.

11. K. L. Kompa and R. D. Levine, ***Proc. Nat. Acad. Sci.*****,** 2001, **98**, 410.

12. G. Favaro, G. Chidichino, P. Formoso, S. Manfredi, U. Mazzucato, and A. Romani, ***J. Photochem. Photobiol. A: Chemistry***, 2001, **140**, 229.

13. F. M. Raymo and S. Giordani, ***Proc. Nat. Acad. Sci.*****,** 2002, **99**, 4941.

14. M. V. Alfimov, O. A. Fedorova, and S. P. Gromov, ***J. Photochem. Photobiol. A: Chemistry***, 2003, **158**, 183.

15. M. Inouye, ***Mol. Cryst. Liq. Cryst.***, 1994, **246**, 169.

16. N. Shao, H. Wang, X.-D. Gao, R.-H. Yang and W.-H. Chan, ***Anal. Chem.***, 2010, **82**, 4628.

17. I. S. Park, Y.-S. Jung, K.-J. Lee and J.-M. Kim, ***Chem. Commun.***, 2010, **46**, 2859.

18. M.-A. Su, T. H. Suzuki, J. Hibino, and Y. Kishimoto, ***Mol. Cryst. Liq. Cryst***., 1994, **246**, 389.

19. J. Andersson, S. Li, P. Lincoln and J. Andre′asson, ***J. Am. Chem. Soc.***, 2008, **130**, 11836.

20. L. Zhu, M.-Q. Zhu, J. K. Hurst and A. D. Q. Li, ***J. Am. Chem. Soc.***, 2005, **127**, 8968.

21. S. Cotton, ***Lanthanide and Actinide Chemistry*** (John Wiley & Sons, Ltd, Chichester, UK, 2006).

22. P. Atkins, T. Overton, J. Rourke, M. Weller, F. Armstrong, and M. Hagerman, ***Inorganic Chemistry*** (W. H. freeman and Company, New York, 2010).

23. W. Koechner and M. Bass, ***Solid-State Lasers - A Graduate Text*** (Springer-Verlag, New York, 2003).

24. G. H. Dieke, ***Spectra and energy levels of rare earth ions in crystals*** (Interscience Publishers, New York, 1968).

25. F. Auzel, ***Chem. Rev.***, 2004, **104**, 139.

26. F. Wang and X. Liu, ***Chem. Soc. Rev.***, 2009, **38**, 976.

27. M. Lin, Y. Zhao, S. Wang, M. Liu, Z. Duan, Y. Chen, F. Li, F. Xu, and T. Lu, ***Biotechnol. Adv.***, 2012.

28. J. F. Suyver, A. Aebischer, D. Biner, P. Gerner, J. Grimm, S. Heer, K. W. Krämer, C. Reinhard and H. U. Güdel, ***Opt. Mater.***, 2005, **27**, 1111.

29. Y.-Y. Huang, M. Hamblin and A. C.-H. Chen, ***SPIE***, 2009, **06**, 1669.

30. V. Mahalingam, F. Vetrone, R. Naccache, A. Speghini and J. A. Capobianco, ***Adv. Mater.***, 2009, **21**, 4025.

31. J.-C. Boyer, C.-J. Carling, B. D. Gates and N. R. Branda, ***J. Am. Chem. Soc.***, 2010, **132**, 15766.

32. *IUPAC Compendium of Chemical Terminology - the Gold Book*; International Union of Pure and Applied Chemistry, 2009

33. S. M. Aldoshin, ***Russ. Chem. Rev.,*** 1990, 663.

34. V. I. Minkin, ***Chem. Rev.,*** 2004, **104**, 2751.

35. A. S. Kholmanskii, K. M. Dyumaev, ***Russ. Chem. Rev.,*** 1987, 136.

36. J. Z. Zhang, B. J. Schwartz, J. C. King and C. B. Harris, ***J. Am. Chem. Soc.,*** 2002, **114**, 10921.

37. N. P. Ernsting and T. Arthen-Engeland, ***J. Phys. Chem.,*** 1991, **95**, 5502.

38. J. O. Morley, R. M. Morley, R. Docherty and M. H. Charlton, ***J. Am. Chem. Soc.***, 1997, **119**, 10192.

39. H. Görner, ***Phys. Chem. Chem. Phys.,*** 2001, **3**, 416.

40. H. E. Simmons and T. Fukunaga, ***J. Am. Chem. Soc.***, 2002, **89**, 5208.

41. P. Maslak, A. Chopra, C. R. Moylan, R. Wortmann, S. Lebus, A. L. Rheingold, G. P. A. Yap, ***J. Am. Chem. Soc.***, 1996, **118**, 1471.

42. P. Maslak and A. Chopra, ***J. Am. Chem. Soc.***, 1993, **115**, 9331.

43. P. Celani, F. Bernardi, M. Olivucci and M. A. Robb, ***J. Am. Chem. Soc.,*** 1997, **119**, 10815.

44. J. Garside, and R. J. Davey, ***From Molecules to Crystallizers***, (Oxford University Press, Oxford, 2000)

45. J. W. Mullin, ***Crystallization***, Fourth Edition (Reed Education and Publication Ltd. Oxford, 2001)

46. J. H. Zeng, Z. H. Li, J. Su, L. Wang, R. Yan and Y. Li, ***Nanotechnology***, 2006, **17,** 3549.

47. R. Scheps, ***Prog. Quant. Electr.***, 1996, **20**, 271.

48. F. Auzel, ***C. R. Acad. Sci. (Paris),*** 1996, **262**, 1016.

49. N. Bloembergen, ***Phys. Rev. Lett.*** , 1959, **2**, 84.

50. F. Auzel, ***C. R. Acad. Sci. (Paris),*** 1996, **263**, 819.

51. P. Held, ***An Introduction to Fluorescence Resonance Energy Transfer Technology and its Application in Bioscience,*** (BioTek Instruments Inc, 2005)

52. M.-Q. Zhu, G.-F. Zhang, C. Li, M. P. Aldred, E. Chang, R. A. Drezek and A. D. Q. Li, ***J. Am. Chem. Soc.***, 2011, **133**, 365.

53. M.-M. Russew and S. Hecht, ***Adv. Mater.***, 2010, **22**, 3348.

54. Z. Tian, W. Wu and A. D. Q. Li, ***ChemPhysChem***, 2009, **10**, 2577.

55. H. Tian and Y. Feng, ***J. Mater. Chem.***, 2008, **18**, 1617.

56. C. Zhang, H.-P. Zhou, L.-Y. Liao, W. Feng, W. Sun, Z.-X. Li, C.-H. Xu, C.-J. Fang, L.-D. Sun, Y.-W. Zhang and C.-H. Yan, ***Adv. Mater.***, 2010, **22**, 633.

57. S. Zhang, Q. Zhang, B. Ye, X. Li, X. Zhang and Y. Deng***, J. Phys. Chem. B***, 2009, **113**, 6012.

58. M.-Q. Zhu, L. Zhu, J. J. Han, W. Wu, J. K. Hurst and A. D. Q. Li, ***J. Am. Chem. Soc.***, 2006, **128**, 4303.

59. P. Li, Q. Peng and Y. Li, ***Adv. Mater.***, 2009, **21**, 1945.

60. C.-J. Carling, J.-C. Boyer and N. R. Branda***, J. Am. Chem. Soc.***, 2009, **131**, 10838.

61. C.-J. Carling, N. Farahnaz, J.-C. Boyer and N. R. Branda, ***Angew. Chem., Int. Ed.***, 2010, **49**, 3782.

62. F. Vetrone, R. Naccache, V. Mahalingam, C. G. Morgan and J. A. Capobianco, ***Adv. Funct. Mater.***, 2009, **19**, 2924.

63. R. Naccache, F. Vetrone, V. Mahalingam, L. A. Cuccia and J. A. Capobianco, ***Chem. Mater.***, 2009, **21**, 717.

64. M. Haase and H. Schäfer, ***Angew. Chem., Int. Ed.***, 2011, **50**, 5808.

65. R. Deng, X. Xie, M. Vendrell, Y.-T. Chang and X. Liu, ***J. Am. Chem. Soc.***, 2011,**133**, 20168.

66. F. Wang, R. Deng, J. Wang, Q. Wang, Y. Han, H. Zhu, X. Chen and X. Liu, ***Nat. Mater.***, 2011, **10**, 968.

67. N. Bogdan, F. Vetrone, G. A. Ozin and J. A. Capobianco, ***Nano Lett.***, 2011, **11**, 835;

68. N. Bogdan, F. Vetrone, Rene′ Roy and J. A. Capobianco, ***J. Mater. Chem.***, 2010, **20**, 7543.

69. A. R. Clapp, I. L. Medintz, J. M. Mauro, B. R. Fisher, M. G. Bawendi and H. Mattoussi, ***J. Am. Chem. Soc.***, 2004, **126**, 301.

70. Y. Wu, X. Qu, L. Huang, D. Qiu, C. Zhang, Z. Liu, Z. Yang and L. Feng, ***J. Colloid Interface Sci.***, 2010, **343**, 155.

71. J. B. Jr. Flannery, ***J. Am. Chem. Soc.***, 1968, **90**, 5660.

72. V. Mahalingam, R. Naccache, F. Vetrone and J. A. Capobianco, ***Chem.-Eur. J.***, 2009,**15**, 9660.

73. V. Mahalingam, R. Naccache, F. Vetrone, J. A. Capobianco, ***Chem. Commun.***, 2011, **47**, 3481.

74. T. Pellegrino, L. Manna, S. Kudera, T. Liedl, D. Koktysh, A. L. Rogach, S. Keller, J. Rädler, G. Natile and W. J. Parak, ***Nano Lett.***, 2004, **4**, 703.

75. H. Wong, F. Vetrone, R. Naccache, H. L. W. Chan, J. Hao and J. A. Capobianco, ***J. Mater. Chem.***, 2011, **21**, 16589.